NUMERICAL AND PHYSICAL SIMULATIONS OF

EFFECT OF MINE OPENING GEOMETRIES ON

SURFACE SUBSIDENCE UNDER

SUB-CRITICAL CONDITION

Thitawee Sooppattagul

A Thesis Submitted in Partial Fulfillment of the Requirements for the

Degree of Master of Engineering in Civil, Transportation

and Geo-resources Engineering

Suranaree University of Technology

Academic Year 2019

การจำลองเชิงตัวเลขและเชิงกายภาพของรูปร่างเหมืองใต้ดินต่อการทรุดตัว
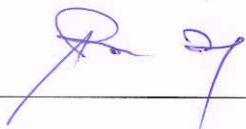## ของผิวดินที่ต่ำกว่าจุดวิกฤต

นางสาวฐิตวี สุพพัตกุล

NUMERICAL AND PHYSICAL SIMULATIONS OF EFFECT OF

MINE OPENING GEOMETRIES ON SURFACE SUBSIDENCE

UNDER SUB-CRITICAL CONDITION

Suranaree University of Technology has approved this thesis submitted in partial fulfillment of the requirements for a Master's Degree.
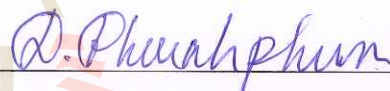
Thesis Examining Committee

_____

(Assoc. Prof. Dr. Pornkasem Jongpradist)

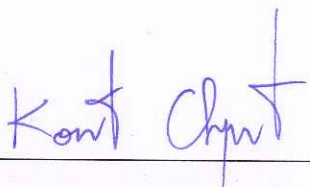Chairperson

_____

(Asst. Prof. Dr. Decho Phueakphum)

Member (Thesis Advisor)

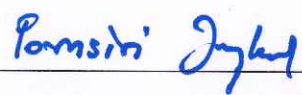_____

(Asst. Prof. Dr. Akkhapun Wannakomol)

Member

_____

(Assoc. Prof. Flt. Lt. Dr. Kontorn Chamniprasart)

Vice Rector for Academic Affairs

and Internationalization

_____

(Assoc. Prof. Dr. Pornsiri Jongkol)

Dean of Institute of Engineering

ฐิตวี สุพพัตกุล : การจำลองเชิงตัวเลขและเชิงกายภาพของรูปร่างเหมืองใต้ดินต่อการทรุด
ตัวของผิวดินที่ต่ำกว่าจุดวิกฤต (NUMERICAL AND PHYSICAL SIMULATIONS OF
EFFECT OF MINE OPENING GEOMETRIES ON SURFACE SUBSIDENCE
UNDER SUB-CRITICAL CONDITION) อาจารย์ที่ปรึกษา : ผศ. ดร. เดโช เผือกภูมิ, 73
หน้า

งานวิจัยนี้ศึกษาการทรุดตัวของผิวดินในสภาวะที่ต่ำกว่าจุดวิกฤตภายใต้ความหลากหลาย
ของรูปร่างช่องเหมืองและคุณสมบัติการเปลี่ยนแปลงรูปร่างของชั้นหินปิดทับ โดยวิธีแบบจำลองเชิง
กายภาพและแบบจำลองเชิงตัวเลข การทดลองเชิงกายภาพใช้เจลสังเคราะห์ในการจำลองชั้นหินปิด
ทับ ผลการจำลองเชิงกายภาพและเชิงตัวเลขมีความสอดคล้องกันเป็นอย่างดีในทุกกรณี โดยพบว่า
องค์ประกอบของการทรุดตัวไม่ได้รับผลกระทบจากรูปร่างของเสาค้ำยัน ภายใต้อัตราการสกัดแร่
และแผงการทำเหมืองเดียวกัน ผลจากการจำลองเชิงตัวเลขพบว่า การทรุดตัวสูงสุดลดลงด้วยการ
เพิ่มขึ้นของระดับความลึก สัมประสิทธิ์ความยืดหยุ่น และความกว้างของเสาค้ำยันกันชน มุมการ
ไหลเพิ่มขึ้นด้วยการเพิ่มขึ้นของความสูงช่องเหมืองและความกว้างของเสาค้ำยันกันชน การเพิ่มขึ้น
ของสัมประสิทธิ์ความยืดหยุ่นทำให้มุมการไหลลดลง ความกว้างของการทรุดตัวเพิ่มขึ้นด้วยการ
เพิ่มขึ้นของความสูงช่องเหมือง ระดับความลึก และความกว้างของเสาค้ำยันกันชน ขณะเดียวกัน
ความกว้างของการทรุดตัวลดลงเมื่อสัมประสิทธิ์ความยืดหยุ่นเพิ่มขึ้น อัตราการสกัดแร่มีผลต่อการ
ทรุดตัวสูงสุดแต่ไม่ส่งผลต่อขนาดของมุมการไหลและความกว้างของการทรุดตัว สมการเชิง
ประจักษ์ที่ได้จากผลการจำลองเชิงตัวเลขสามารถใช้คาดคะเนองค์ประกอบการทรุดตัวของผิวดิน
เหนือแผงการทำเหมือง

สาขาวิชา เทคโนโลยีธรณี   ลายมือชื่อนักศึกษา _____
ปีการศึกษา 2562   ลายมือชื่ออาจารย์ที่ปรึกษา _____

THITAWEE SOOPPATTAGUL: NUMERICAL AND PHYSICAL
SIMULATIONS OF EFFECT OF MINE OPENING GEOMETRIES
ON SURFACE SUBSIDENCE UNDER SUB-CRITICAL CONDITION.
THESIS ADVISOR : ASST. PROF. DECHO PHUEAKPHUM, Ph.D., 73 PP.

PILLAR SHAPE/ TROUGH VOLUME/ EXTRACTION RATIO/ STIFFNESS

Physical and numerical simulations are performed to investigate the sub-critical surface subsidence under a variety of opening geometries and deformation properties of overburden. The synthetic gel is used to simulate the overburden in physical tests. The physical model results agree well with those obtained from numerical simulations for all conditions. The results clearly show that subsidence components are not affected by pillar geometries under the same extraction ratio of the same panel. The numerical analysis results indicate that the maximum subsidence (S_{max}) decreases with increasing opening depth, elastic modulus and abutment pillar width. The angle of draw increases with increasing opening height and abutment width. The increasing of elastic modulus reduces angle of draw. The subsidence trough width (B) increases with increasing opening height and depth, and abutment width, while decreases with increasing elastic modulus. The S_{max} is sensitive to the extraction ratio, but γ and B are not. The empirical equations obtained from computer simulation results can be used to predict the surface subsidence components above the panel.

School of Geotechnology

Academic Year 2019

Student's Signature _____

Advisor's Signature _____

ACKNOWLEDGMENTS

TABLE OF CONTENTS

Page

TABLE OF CONTENTS (Continued)

TABLE OF CONTENTS (Continued)

Page

LIST OF TABLES

LIST OF FIGURES

LIST OF FIGURES (Continued)

LIST OF FIGURES (Continued)

LIST OF FIGURES (Continued)

SYMBOLS AND ABBREVIATIONS

γ	=	Angle of draw
ν	=	Poisson's ratio
B	=	Subsidence trough width
D	=	Opening depth
E	=	Elastic modulus of the overburden
e_a	=	Area extraction ratio
e_v	=	Volumetric extraction ratio
H	=	Pillar height
L	=	Length of panel
S_{max}	=	Maximum subsidence
W	=	Width of panel
W_{ab}	=	Abutment pillar width
W	=	Width of panel
W_m	=	Mine area width
W_o	=	Opening width
W_x	=	Pillar width in x axis
W_y	=	Pillar width in y axis
V_c	=	Opening closure volume
V_s	=	Surface subsidence volume

CHAPTER I

INTRODUCTION

1.1   Background and rationale

Subsidence can induce damage to structures, buildings, railways, environment and ground surface. The subsidence can be caused by natural or artificial activities, such as underground mining, groundwater pumping and tectonics. Subsidence from the mining process that does not exceed the critical point, referred as sub-critical condition.

The combination of physical and numerical model has been demonstrated to be effective for investigating the mechanism of subsidence (Ghabraie et al., 2015). Physical models use scaled down to simulate, as case study, the surface subsidence mechanisms with a limit set of parameters. Numerical models can evaluate ground settlement from various geometries of mine opening and material properties of the overburden. This method is widely used to predict subsidence and economic to estimate subsidence (Reddish, 1989; Alejano et al.; 1999, Shahriar et al., 2009). Most researchers have been focused on the effect of mine depths (Thongprapha et al., 2015), mining sequences and excavation rates (Saoanunt and Fuenkajorn, 2015), overburden properties, opening width and geometries (Sartkaew and Fuenkajorn, 2016). Even though the opening geometries have been varied to simulate subsidence characteristics, but the effect of pillar geometries in a mine panel and extraction ratios have rarely been attempted. To correlate the pillar geometries in mine panel and extraction ratios with the subsidence parameters, their mathematical relationship for predicting the subsidence is needed.

1.2   Research objectives

The objective of this research is to determine the maximum subsidence, angle of draw, subsidence trough as affected by mine panel characteristics by using numerical simulation and physical model under sub-critical condition. SolidWorks and Phase2 are used to simulate the surface subsidence as affected by mine opening geometries, overburden properties, extraction ratios and opening depths. The synthetic gel represents elastic behavior of the overburden used in the physical model. The results from the physical model are compared with those of the computer simulation to assess the accuracy of the test results. The results are used to develop the mathematical relationship between the subsidence parameters and characteristics of underground openings. A set of these equations can be used to predict the surface subsidence components induced by the underground opening under various mine opening geometries.

1.3   Scope and limitations

The scope and limitations of the study include as follows.

1) Physical model used the trap door apparatus (Thongprapha et al., 2015) to simulate the sub-critical surface subsidence.

2) Synthetic gel is prepared to simulate the overburden.

3) The material is 920 kg/m^3 of density and 8.31 kPa of elastic modulus.

4) Opening widths in the physical model are constant at 86 mm. The opening depth is 100 mm. The opening length is 380 and height is 20 mm.

5) Three geometries of pillar shape are used in the physical model at extraction ratio of 50%.

6) Physical model results are compared with numerical simulations.

7) SolidWorks and Phase2 are used in the numerical simulation.

8) Extraction ratios in numerical simulation vary from 40%, 50% to 60%. Six shapes of pillar are simulated in computer models. The opening height is varied from 2, 4, 6, 8 to 10 m, mining depth is selected from 100, 150, 200, 250 to 300 m and elastic modulus of overburden is simulated from 5, 10, 20 to 30 GPa.

9) The experiments are interested on the maximum subsidence, angle of draw, subsidence trough volume and opening closure volume which occurring due to extraction.

1.4 Research methodology

The methodology of research comprises 8 steps; including literature review, material preparation, test frame, physical and numerical simulations, analysis and comparisons, development of mathematical relationships, discussions and conclusions, and thesis writing (Figure 1.1).

1.4.1 Literature review

Literature review is performed to study researches on subsidence in northeastern region of Thailand, sources of information are from journals, reports conference papers and books. A summary of literature reviews is given in this study.

1.4.2 Material preparation

The synthetic gel is prepared to simulate the overburden in physical model test. The major factor of the material used to simulate the overburden is non-toxic and

universally obtainable. Physical properties of the overburden are independent on variations of humidity and temperatures.
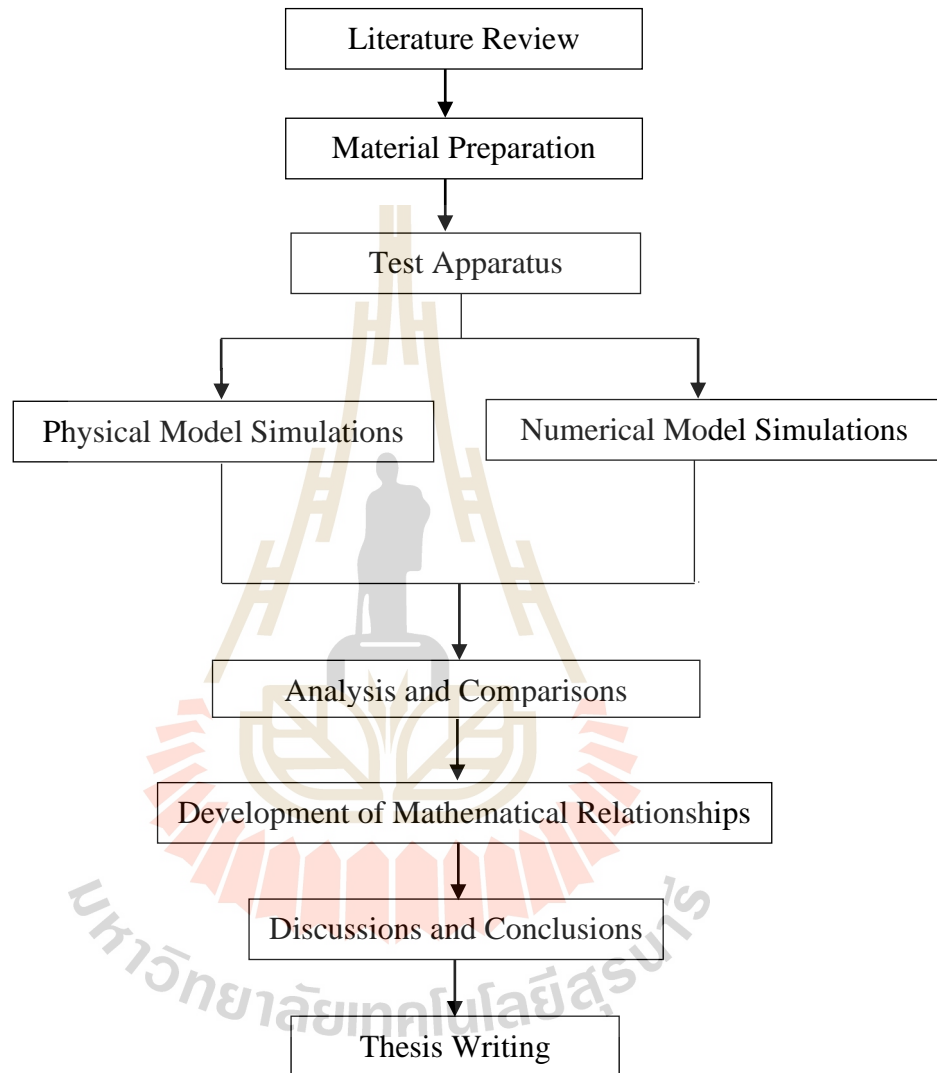
Figure 1.1 Methodology of research

1.4.3 Test apparatus

A trap door apparatus is used to simulate surface and to evaluate the effect of mine opening geometries on the surface subsidence. The testing space is $90.6 \times 40 \times 20$ cm^3. The mine opening simulator is an array of plastic blocks with sizes of $10.75 \times 20 \times 38$ mm^3, $14 \times 20 \times 38$ mm^3, $21.5 \times 20 \times 38$ mm^3, and $43 \times 20 \times 38$ mm^3. The plastic blocks can be systematically and gradually moved down to simulate the underground openings with three different geometries. The laser scanner is used to measure surface of the material before and after the overburden deformation is induced.

1.4.4 Physical model simulations

The physical models are used to simulate subsidence of overburden. The varied parameter are width and length of pillars of the underground openings. The laboratory testing is measured the maximum magnitude of subsidence at critical point (S_{max}) and the angle of draw allowing to study the effect of mine opening geometries or shape of pillar.

1.4.5 Numerical model simulations

The computer programs are used to simulate the characteristics of the subsidence model by considering the effects of pillar geometries and height, mining depth and material overburden properties. The simulations use SolidWorks and Phase2 programs.

1.4.6 Analysis and comparisons

The physical simulation results are compared with the results obtained from numerical simulations (SolidWorks programs) in terms of the maximum surface subsidence and angle of draw.

1.4.7 Development of mathematical relationships

The results from the numerical simulations are used to develop mathematical equations between the subsidence parameters with opening heights and depths, extraction ratios, overburden properties.

1.4.8 Discussions and conclusions

All study methods, and results are documented and approved in the thesis. The research is published in the conference proceedings or journals.

1.5 Thesis content

This thesis is divided into five chapters. **Chapter I** explains the objectives, problems and rationale, and methodology of research. **Chapter II** describes results of the literature review to improve the knowledge of surface subsidence. **Chapter III** describes design fabrication of the test frame, material preparation and test results **Chapter IV** describes the numerical model method, boundary condition to simulate and mathematical relationships. **Chapter V** proposes discussions, conclusions and recommendation for future studies.

CHAPTER II

LITERATURE REVIEW

2.1 Subsidence in northeastern region of Thailand

The northeastern Thailand is in the Khorat Plateau and divided to the northern Sakhon Nakhon Basin and the southern Khorat Basin (Figure 2.1). Two basins performed claystone and rock salt layers of Maha Sarakham Formation

The rock salt underneath subsurface in the Sakon Nakhon Basin has an area approximately 20,323 km^2, covering the area of Udon Thani, Nong Khai, Sakon Nakhon, Mukdahan, Nakhon Phanom, and some part of Laos, and the Khorat Basin has an area about 25,620 km^2, covering the province of Khon Kaen, Nakhon Ratchasima, Chaiyaphum, Kalasin, Roi Et, Maha Sarakham, Ubon Ratchathani, Burirum, Yasothon, Sisaket and Surin (Satarugsa et al., 2005).

Salt productions from brine (saline groundwater) are found in the Khorat and the Sakhon Nakhon Basin. Brine groundwater well depth is about 60 to 100 meters. The brine is pumped to ground surface for solar evaporation, this technique known as the 'brine-pumping' method. Based on field investigation (Wannakao et al., 2005) and Jenkunawat (2007) states that the ground surface subsidence usually occurs in areas where the depth is less than 50 meters. Investigation results, claystone at ground surface, the salt dome located under the salt production zone at depth about 40 to 50 meters. Rock salt was located at depth 40 to 200 meters. Gypsum and anhydrite were observed nearby the salt dome. Sinkholes are circular shapes, with diameter approximately 50 to 100 meters. Surface subsidence normally starts at pumping well and moves in a

sequences of surface subsidence. They occur in only salt dome in brine zone, fractures and salt dissolution. However, the brine pumping method is inexpensive and simple, but this method can be caused an environmental impact in the form of unpredictable ground movement, surface contamination and sinkholes (Fuenkajorn, 2002).
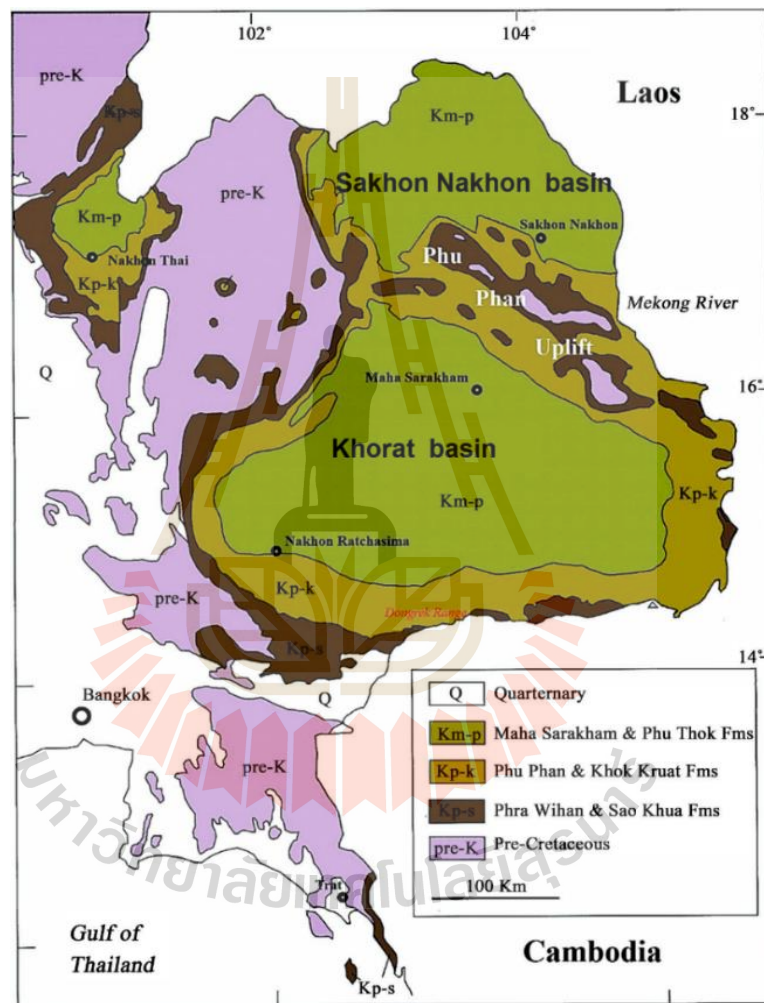
Figure 2.1 Khorat and Sakon Nakhon basins (modified from Meesook, 2011).

2.2   Theory and Criteria

Subsidence is ground settlements that occur due to overlying strata collapse into mining void. The area of disturbed land surface over a collapsed mine is called the subsidence trough (Singh, 1992; Hawkes, 2010) based on panel extraction width, extraction area and mining depth be categorized include subcritical, critical and super-critical width. Figure 2.2 to 2.4 show the horizontal ground surface over horizontal coal seam. Two dimensions are considered. A coal seam portion has been extracted, resulting in a subsidence trough at the ground surface. For simplicity, the parameters h and m (and therefore the parameters S_{max} and B) are taken as constants in each figure. The subsidence factor (a) is taken to be 1.0 then that calculated maximum surface subsidence (S_{max}) is equal to the overburden depth or thickness (m). Figure 2.2 represents a sub-critical subsidence where the mining extracted width is less than 2·B, Figure 2.3 represents a critical subsidence, where the mining extracted width is equal to 2·B and Figure 2.4 represents a super-critical subsidence where the mining extracted width is larger than 2·B. The maximum amount of subsidence is equal to the calculated value of S_{max} above a finite distance over the center of the mine extraction area, start at a distance B from the edge of the extraction area.

The major objectives of surface subsidence engineering are predicted of surface displacement, determined the effects of such movements on structures and minimized damage of surface subsidence.
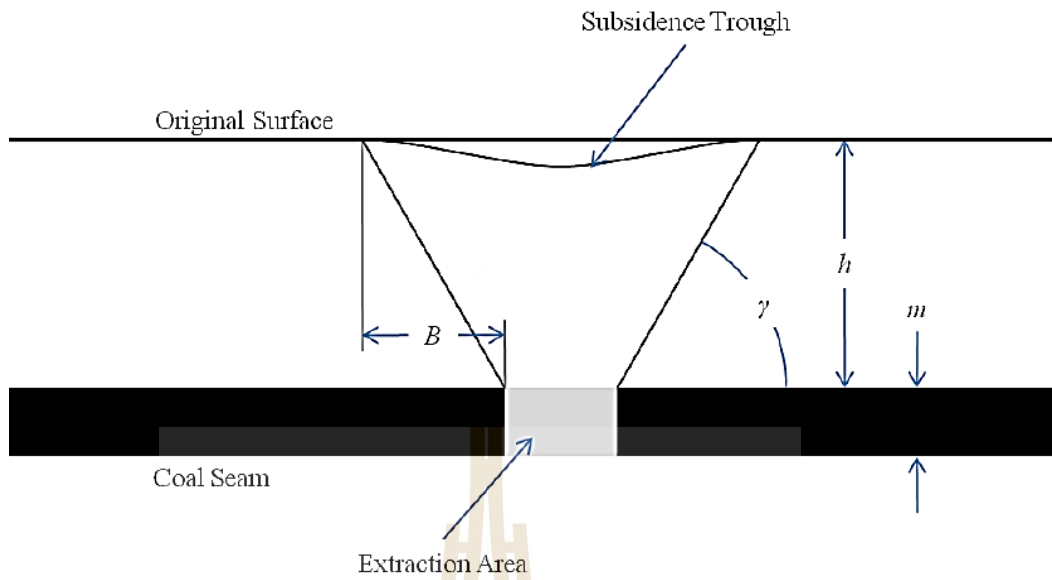
Figure 2.2 Sub-critical extraction (Hawkes, 2010).
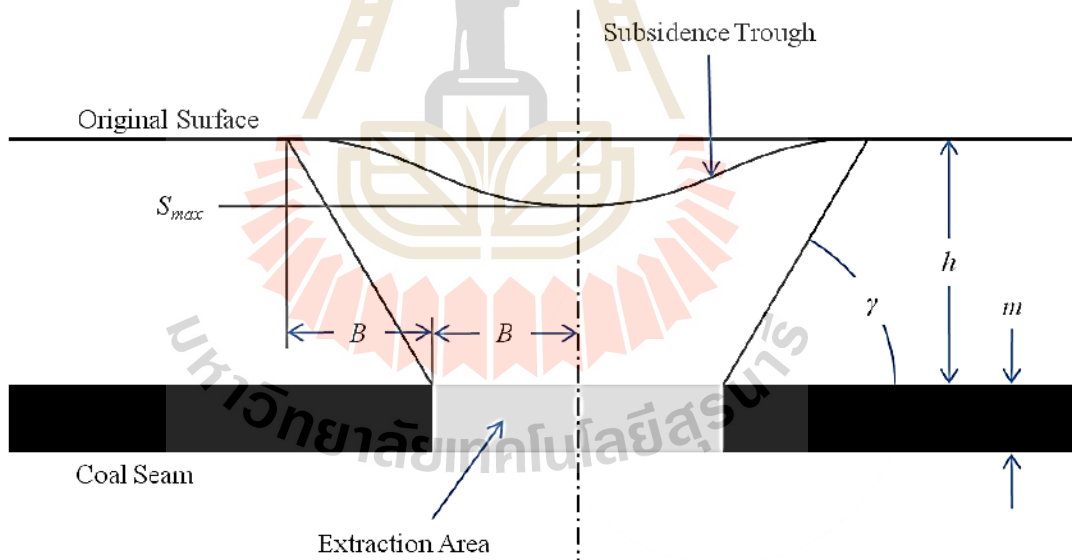
Figure 2.3 Critical extraction (Hawkes, 2010).
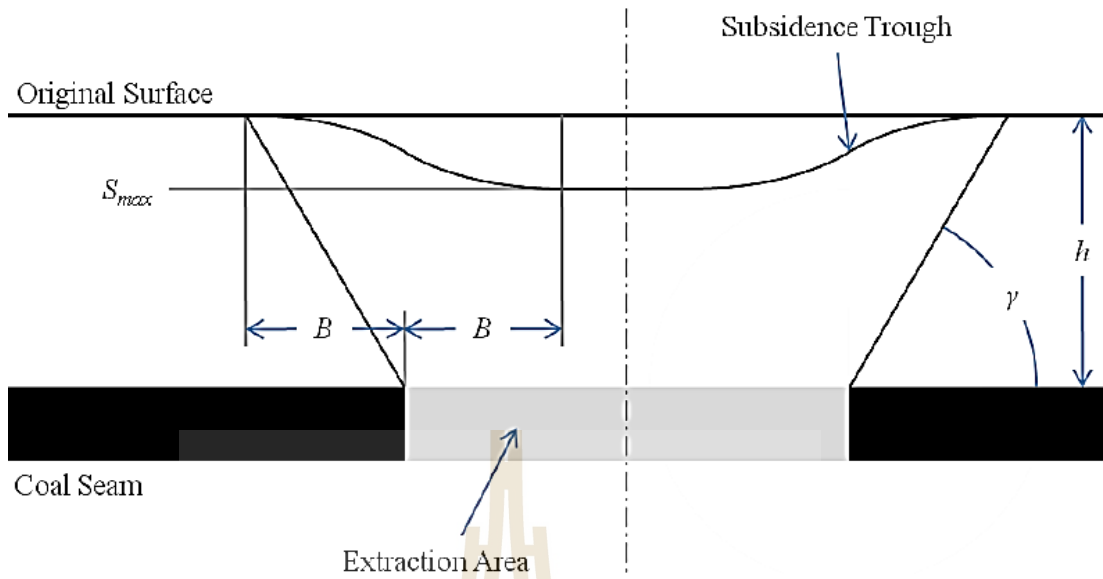
Figure 2.4 Super-critical extraction (Hawkes, 2010).

Subsidence consists of five major components are vertical movement, lateral movement, tilt, vertical strain and curvature, as follows;

Vertical movement:

$$S(x) = \frac{1}{2} S_{max} \left[1 - \tanh\left(\frac{cx}{B}\right) \right] \tag{2.1}$$

Tilt (or slope):

$$G(x) = S'(x) = -\frac{1}{2} S_{max} \frac{c}{B} \operatorname{sech}^2\left(\frac{cx}{B}\right) \tag{2.2}$$

Vertical curvature:

$$\rho(x) = S''(x) = S_{max} \frac{c^2}{B^2} \left[\operatorname{sech}^2\left(\frac{cx}{B}\right) \tanh\left(\frac{cx}{B}\right) \right] \tag{2.3}$$

Lateral movement (horizontal displacement):

$$u(x) = -\frac{1}{2}S_{max}\frac{bc}{B}sech^2\left(\frac{cx}{B}\right)$$

(2.4)

Lateral strain:

$$\varepsilon(x) = S_{max}\frac{bc^2}{B^2}\left[sech^2\left(\frac{cx}{B}\right)tanh\left(\frac{cx}{B}\right)\right]$$

(2.5)

where S_{max} = the maximum surface subsidence,

D = the opening or cavern depth,

B = cavern maximum radius,

γ = angle of draw,

c = constant,

b = constant,

x = horizontal distance

2.3   Physical modeling

Physical models are useful for understanding mechanism of subsidence (Whittaker and Reddish, 1989; Alejano et al., 1999; Asadi et al., 2005). It allows deformation to occur by natural mechanisms which can be compared to numerical simulations and field observations. Processes such as ground surface movements, crack propagation caving and underground displacements.

Physical model simulations are performed for study behavior of the prototypes. Most of physical model simulations are constructed small scales because the test results

are expected to obtain more promptly and with closer control over model details than the full-scale testing.

Ghabraie et al. (2017) study the multi-seam mining induced ground subsidence profile and compared with single-seam mining. Knowledge of the characteristics of multi-seam settlements are the first step in accomplish reliable ground surface movement predictions. Multi-seam subsidence characteristics are investigated by physical models. Several measurement tools were used to monitor surface subsidence parameters, these include Optical Non-contact Displacement Transducers (optpNCDT), Terrestrial Laser Scanner (TLS), and a digital camera. The models perform and these devices are illustrated in Figure 2.5. Model results show that the multi-seam mining area can be divided to different zones. Each zone shows specific surface subsidence characteristics according to super-positioning and relative location of panels in the two seams. This research can define the effects of underground mining configuration on the multi-seam surface subsidence parameters and supports judging the effects of the multi-seam on surface subsidence.

Saoanunt and Fuenkajorn (2015) present the effects of the mining sequences, overburden slope and excavation rates on super-critical subsidence by using trap door apparatus. They found that the angle of draw and S_{max}/H ratios decrease with increasing Z/H ratios when the mining height (H) is maintained constant at 50 mm and the mining depth (Z) varies from 50 mm to 200 mm. In order to mining sequence from the center of panel gives the lowest angle of draw and highest settlements while excavation from the edge to center of panel is causing the highest angle of draw and the lowest

subsidence. Under various overburden slopes, the angle of draw on up-slope and down-slope increases with increasing slope angles. The S_{max}/H ratios decrease with increasing Z/H ratios and slope angles. The results can be used to estimate the surface profile for various underground excavation methods as affected by excavation sequence, overburden slope and extraction rate in a heavily fractured rock mass.
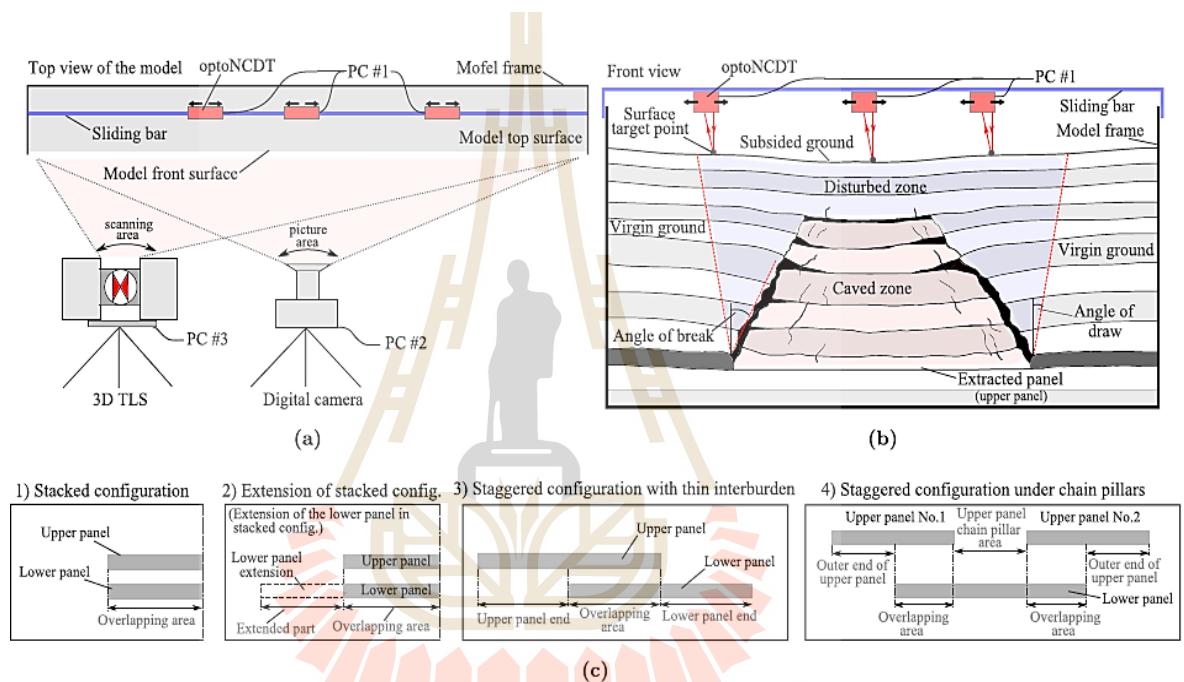
Figure 2.5 Top view(a) and front view (b) of the model construct and measurement tools, (c) multi-seam configurations modelled (Ghabraie et al., 2017).

Meguid et al. (2008) study the physical modeling of the soft ground tunnels is a necessary of the analysis and design of the tunnels. Physical model simulations can be provided data that can calibrate and validate numerical simulations. For many decades, many worldwide researchers have implemented and developed a diversity of technics to simulate the underground excavation process. However, it not accurately simulates the in-situ stress conditions. Centrifuge testing makes more realistic simulation of field stresses possible, but the tunnel construction process has to be simplified. Other approaches have been developed to simulate the system of soft ground tunnel construction. Vertical stresses as well as surface movements can be determined by lowering the trap door apparatus under 3D or 2D conditions. The tunnel face stability can be determined using flexible membrane at the face and rigid tube. Tunnel excavation is simulated by monitoring the soil movements and reducing air pressure inside the tunnel. Different methods comprise the polystyrene core show some success; but the tunnel excavation induced ground subsidence is non-uniform.

Caudron et al. (2006) found that physical models allow to present a case study and to define it absolutely with limited set of parameters. They study interaction of soil in a sinkhole phenomenon using analog 2D physical model (Figure 2.6) and numerical simulation. The material in simulations is used the bi-dimensional Schneebeli material.

Figure 2.6 Small-scale experimental model (Caudron et al., 2006).

Asadi et al. (2005) suggest new profile function. It is formed from the sum of two exponential functions that have been modified to three survey lines in the case study in the Negin coalmine east of Iran. Because of simplicity of profile function, the using new model reduces the calculation time for predicting the land surface subsidence and improves the precision of subsidence prediction. The results obtained from ground movement measurements at Negin coalmine show a good correlation between the predicted and measured the ground subsidence by using the new model. The coefficient of correlation is 0.999, that is extremely high. In the empirical relationships, different tables and graphs are given for different geometrical shapes and conditions. It is possible to predict amount of the subsidence using these tables and graphs. The

National Coal Board (NCB) has recommended one of the most well-known graphs for the prediction of surface subsidence (Figure 2.7).

By clear monitoring and processing of data, the amount of ground surface movement in a real condition is calculated. The example of the physical model as shown in Figure 2.8. In numerical model methods, subsidence and movements of ground surface can be calculated by using boundary elements, finite elements, finite difference and distinct elements methods. Computer application for solved complex of equations in differing initial and boundary conditions with different material behavior made the numerical model methods more popular in the surface subsidence prediction. Other program has been developed to consider anisotropic and inhomogeneous behavior of rock mass worldwide.
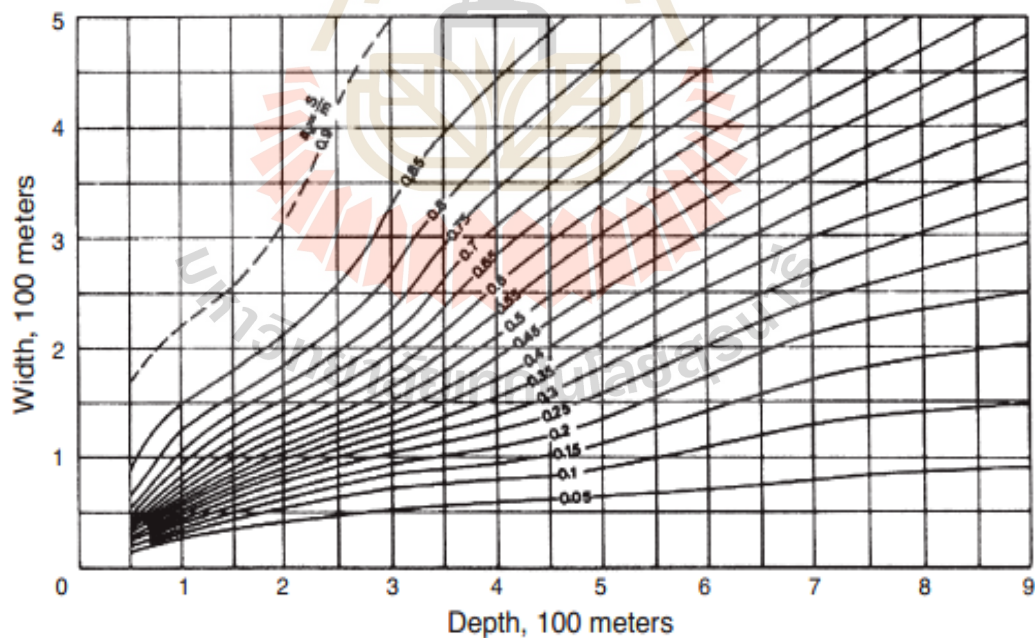
Figure 2.7 Graph suggested by NCB (Asadi et al., 2005).
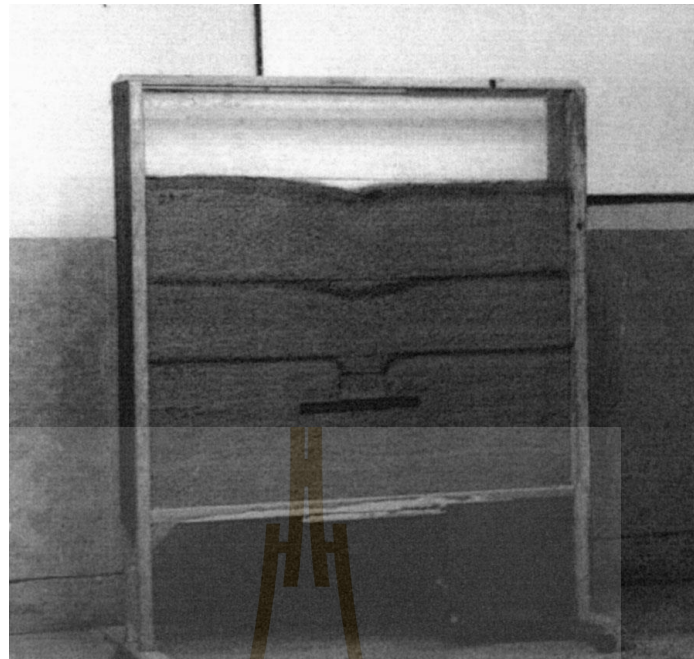
Figure 2.8 A physical model for prediction of subsidence (Asadi et al., 2005).

Park and Li (2004) conclude that surface movement causes damage for example the deterioration and failure of infrastructures, buildings, underground utility lines, dams, etc., resulting in environmental hazards and severe economic loss. The main cause of surface movement is underground mining activities. For reduce and prevent surface subsidence damage, it is necessary to understand surface movement phenomena. It is difficult to predict or simulate ground surface subsidence development because of the complexity in physical characteristics (e.g. rock behavior, time dependent behavior and dimensional variations). In this research a new physical surface subsidence modeling technic is introduced. The method uses laser optical triangulation distance measurement tools, it can scan the surface of any material, including viscous or granular materials, and digitally measure vertical distances with a high resolution and accuracy. With this new technique, the effects of cavity size and shape, depth, and material properties can be analyzed. Using this unique method and technology of

analysis, valuable results were produced. Subsidence profiles and factors, and angles of draw were analyzed. This study is being continued using the same technique for simulated surface subsidence with different model materials for various underground opening configurations and time dependent subsidence phenomena.

2.4   Numerical modeling

Numerical models have more advantage than physical models in terms of cost and time. However, the numerical model is an accurate reflection of physical reality.

The numerical method composes of continuum and discontinuum modelling are useful tool for predicting surface subsidence. The finite difference method (FDM) is mostly used because of simplicity and the possibility of handling the non-linear behavior, but FDM was limited to regular mesh and was not capable of simulating irregular geometries and complex boundary conditions. The finite element method (FEM) mostly used among of the numerical method because of its capabilities to present heterogeneous material, nonlinear behavior such as plasticity, complex geometries and boundary conditions. The boundary element method (BEM) is to perform fracturing in rocks because of the most recent formulations, to reduce the problem complexity from 3D to 2D, or 2D to 1D and solve the problem at boundary. It is suitable for solving large scale problems. The distinct element method (DEM) solves the motion equations and allows de-bonding and detaching of elements, it is represented true discontinuities and suitable for problems with large number of fractures which are outstanding in failure process. (Nikolić et al. 2016)

Rajabi (2018) compares between land subsidence from numerical model by using PLAXIS 3D with satellite image by using InSAR (from the ASAR; Envisat satellite) in some parts of the Qom plateau, Aliabad plain, Iran. The model results agree

well with the results obtained from InSAR by other researchers, both showing an approximately equal surface subsidence in 12 years ago, as shown in Figure 2.9.

Tajduś (2015) studies the numerical simulations and modeling of mining-induced ground surface movement based on the FEM. Numerical method applying discuss to calculations allows us to assume many factors (e.g. rock mass structure, rock properties, etc.), which importantly affect the results obtain. Based on the elastic transversely isotropic model, the analysis of lateral displacement distribution and ground movement is carried out for mining area. The numerical simulation results are compared with the measured values. The calculation results of surface displacement, tilt and lateral displacement are presented and compared with the surveying measurement data, as shown in Figure 2.10 and the influence of changes of the Poisson's ratios, the results show that increase of the Poisson's ratio causes the increase of maximum subsidence and horizontal displacements (Figure 2.11).
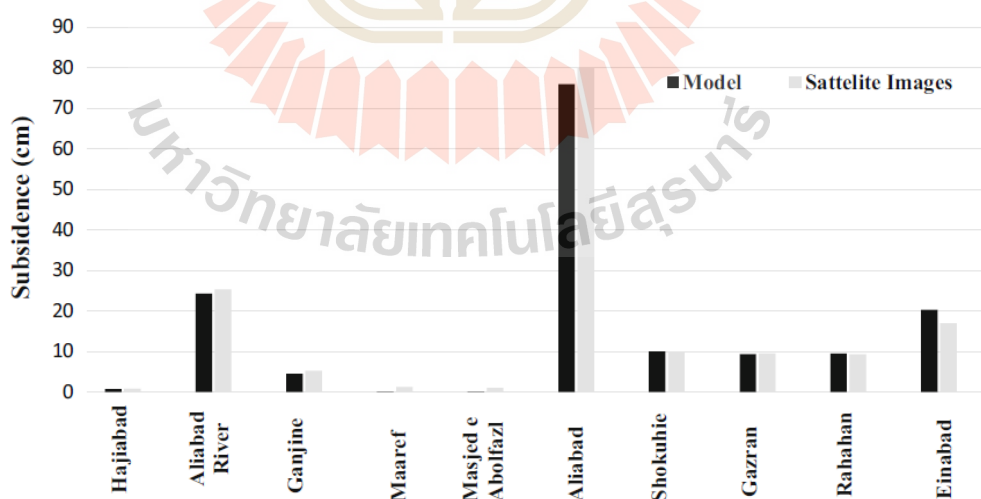
Figure 2.9 Comparison of the results of the numerical model and satellite images

(Rajabi, 2018).
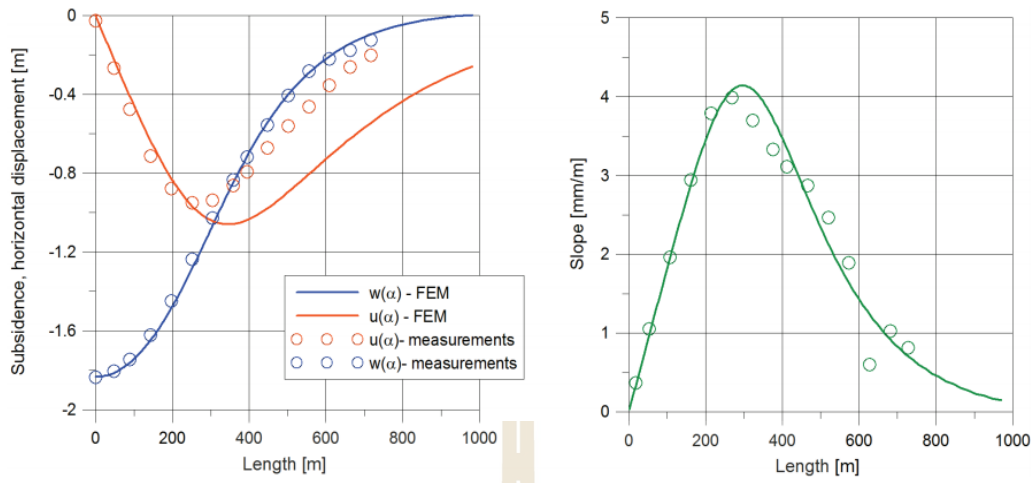
Figure 2.10 Comparison of subsidence, lateral displacement and tilt (slope) for

surveying measurement with FEM (Tajduś, 2015).
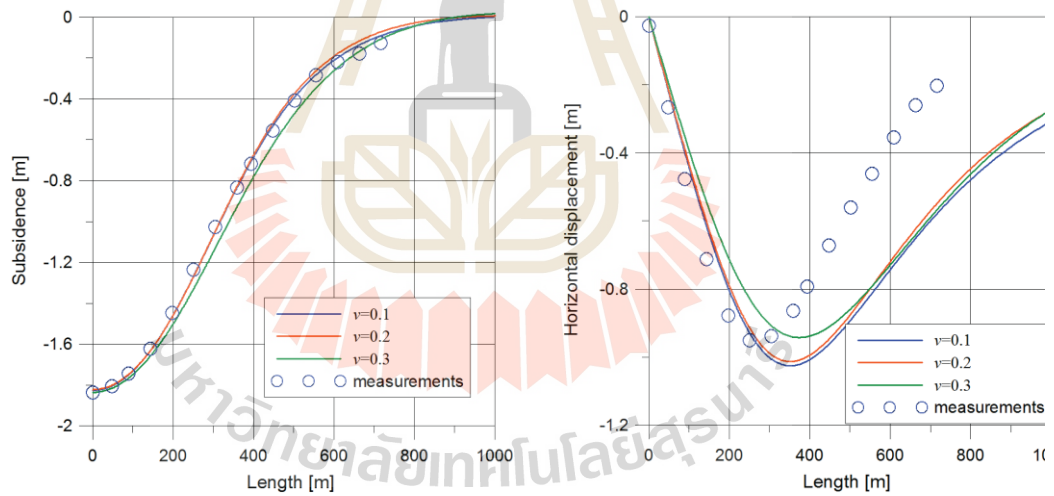
Figure 2.11 Subsidence and lateral displacement under various the Poisson's ratio

(Tajduś, 2015).

Parise and Lollino (2011) observe the computer model simulations that natural cavities represent potential environmental damage, owing to the occurrence of instability within caves, which may spread upward and eventually reach the ground surface, inducing the sinkhole occurrence. They analyzed the failure mechanisms observed in the field for subsurface instability systems and the factors that seem to influence the systems. Computer models were done using both the distinct element method for jointed rock mass conditions and the FEM for geological settings represented by continuous soft rock mass. Both the effects of local instability processes occurring underground and the effects of the progressive enlargement of the caves on the overall stability of the rock mass were investigated including the consequent failure mechanisms.

Wu et al. (2010) study surface settlement caused by groundwater over-pumping in Shanghai is becoming a serious geological hazard, because its important economic location, the field data along with the individual stratum compression from extensometers and groundwater heads from observation wells, have been recorded more than 45 years ago. Considering the fact that different hydro-stratigraphic units have different deformation types and that an identical unit may also present different deformation characteristic (e.g. elasticity, viscoelastoplasticity and elastoplasticity) at different sites of the cone of different periods or depression in, a non-linear coupled regional land subsidence models are developed. The coupled model comprises of a 3D groundwater flow model and a 1D vertical deformation model, both based on a viscoelastoplastic constitutive laws and then solved using a multiscale iterative finite-element method (MsFEM). The model is calibrated using 26,732 deformation measurements 28,184 and hydraulic head measurements from 1961 to 2005 as shown in

Figure 2.12. The calibrated and estimated models are then used to evaluate the future evolution of surface subsidence under 2 groundwater pumping scenarios. Predicted results suggest that restricting groundwater pumping is effective in reduced the annual surface subsidence rate. Furthermore, the average cumulative ground movement from 2006 to 2020 can be controlled less than 40 mm when the groundwater pumping rate is reduced to 25 million cubic meters per year. Even though the area affected by land subsidence continues to enlarge and cumulative of ground movement stills continue to increase because of the deformation delay.
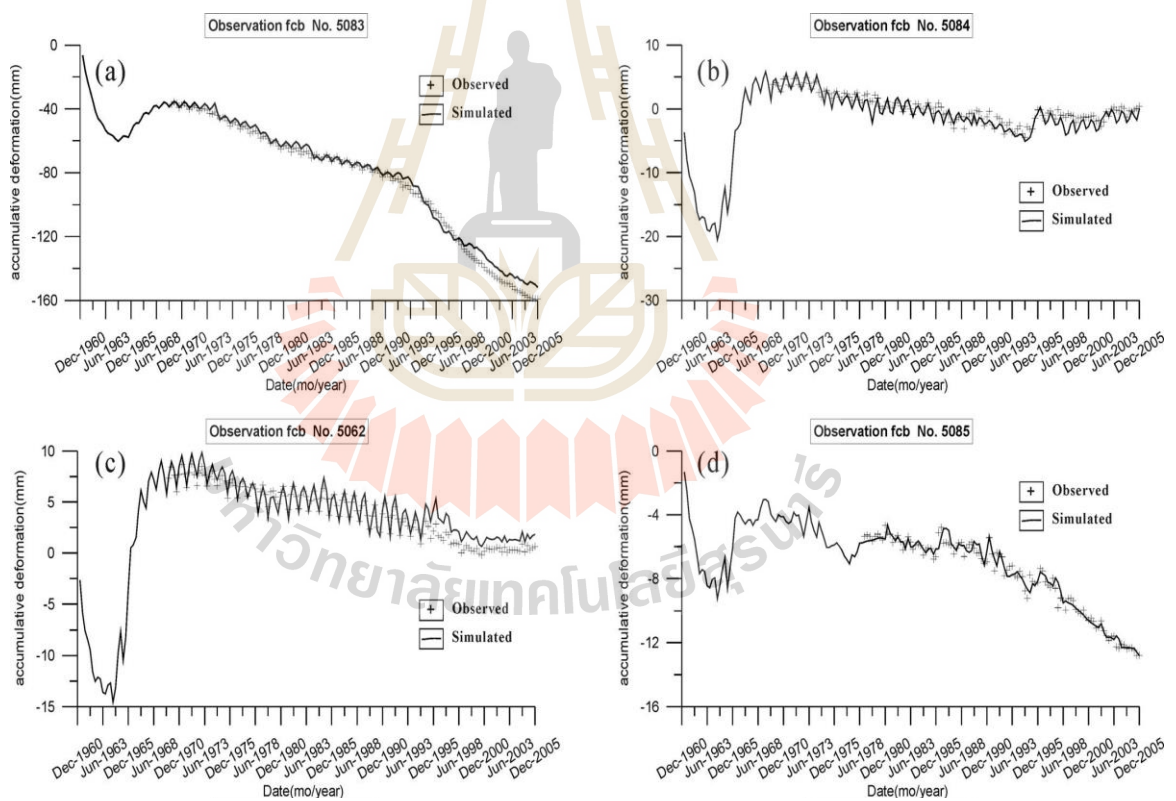
Figure 2.12 Comparison accumulative deformation between measured and simulated

deformation (Wu et al., 2010).

Fuenkajorn and Archeeploha (2010) develop an analytical method to evaluate the location, size and depth of the caverns created at the interface between salt and overlying formations. The hyperbolic function is used in the survey data statistical analysis to determine the cavern location, maximum surface settlement, tilt or slope, and curvature under subcritical and critical conditions. The computer program is developed to execute the regression and produce a set of surface subsidence components and a representative profile of the surface subsidence. Finite difference analyses (FDM) using FLAC correlate the surface subsidence components with the cavern size and depth under the variety of overburden strengths and deformation moduli (Figure 2.13). The empirical equations correlate subsidence components with the cavern configurations and overburden properties. For the super-critical condition, a discrete element method (DEM) using UDEC software is used to simulate the uncertainties of the sinkhole development and ground movement resulting from the joint movement complexity and overburden post-failure deformation. The correlations of the subsidence components with the cavern geometries and overburden properties are applicable to the range of actual conditions especially assigned here (e.g., half oval-shaped cavern created in overburden-salt interface, flat ground surface, saturated condition, and horizontal rock units). These equations may not be applicable to surface subsidence induced under different configurations of the caverns or different rock characteristics. The method is not applicable under super-critical conditions where post-failure behavior of the overburden is unpredictable and complicated by the joints system, as simulated by the results of DEM analyses. The method is useful as predictive tool to

determine the configurations (size and depth) of a salt solution cavern and the ground

surface subsidence components induced by the brine pumping method.
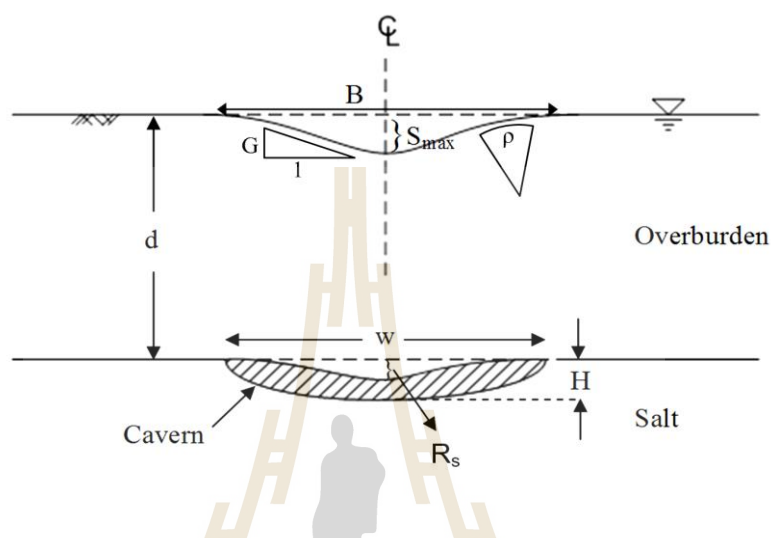
Figure 2.13 Variables used by Fuenkajorn and Archeeploha (2010).

Shahriar et al. (2009) study the ground surface movement due to inclined

extremely shallow coal mining in Parvadeh (Tabas) coalfield. They are using FLAC3D

software which is based on FDM. The FDM results were compared with the field

observed profile and profile function method. FDM underestimated maximum

subsidence up to 3% in comparison with surveying and profile function. The rationale is

the residual surface subsidence is neglected in this study, but the profile function

method predicts last surface subsidence trough. Additionally, in both cases, FDM in

contrast with the measured profiles obtained by profile function and surveying,

predicted uplift above the panels rise side at ground surface in which was verified by

local serveying. The reason that no uplift was observed in the measured profile

contributed by Shahriar et al. (2009) and Asadi et al. (2005) were attempts just have

been focused on measuring downwards surface settlement. The location of maximum surface subsidence in shallow coal seams moved towards the panel rise side which was totally in contrast with the deep seam. Sensitivity analysis indicated that by increased of the mining depth, this point gradually moves toward the panel dip side (Figures 2.14 and 2.15). It was also concluded that critical width to opening depth ratio (W/H) range is varied of 1.0 to 1.4 for both panels. This range is a little lower than the critical range W/H ratio which has been defined by the National Coal Board of UK (1975). This may be related to extremely low depth situation of both panels. Numerical model simulations can demonstrate surface subsidence mechanism better than the profile function caused taking into accounts the geo-material mechanical properties. The profile function results can rarely be extrapolated from the one coal mining area to different area. Empirical methods have their own advantageous cause of inexpensive and simple applications.
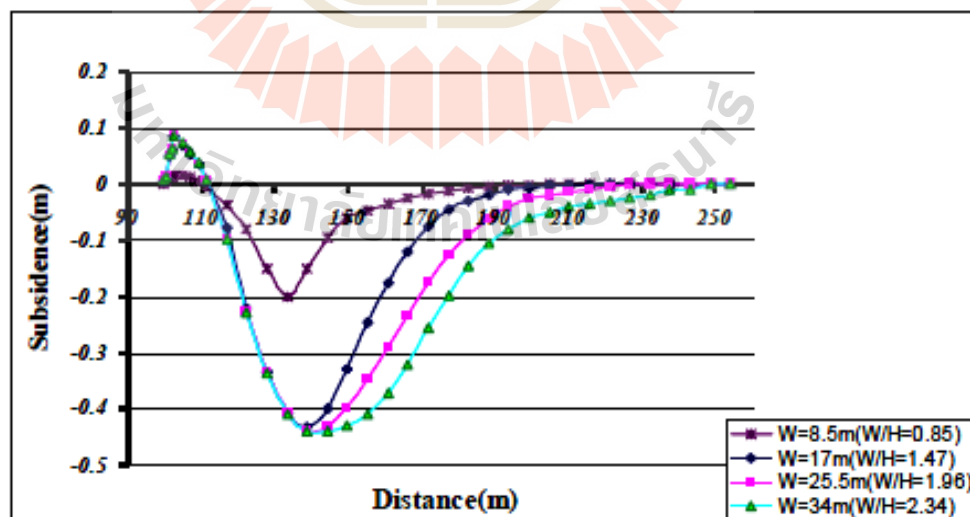
Figure 2.14 Sensitivity analysis on panel width (Shahriar et al., 2009).
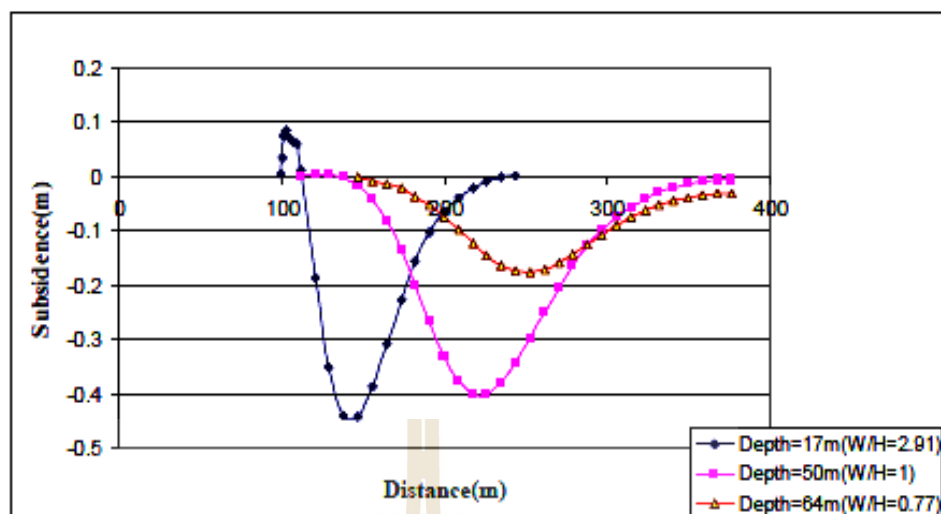
Figure 2.15 Sensitivity analysis on seam depth (Shahriar et al., 2009).

Ren and Li (2008) investigate the mining subsidence extent affected area is described by the limit angles or angles of draw, which is controlled by the mining configurations and geological conditions of the overburden, including seam inclination angle. From observed worldwide data and numerical modeling analysis can conclude that the strength, stiffness and overburden failure play important role in the limit of surface subsidence characteristics. When overburden rocks are satisfactorily strong and no roof failure, the limit angle tends to be greater in roof rocks with higher stiffness. However, if collapses of the roof, the stronger overburden would develop the lower limit angle at the ground surface and weak roof overburden would result in the greater limit angle. When there is a sufficiently stiff and strong of the overburden, it is probable for a sub-critical subsidence profile to be improved above a panel of super-critical width. The rock stiffness and strength also affect the maximum subsidence. Normally, the maximum surface subsidence over a weak overburden is more than that over a strong overburden. The FEM model shown in Figure 2.16
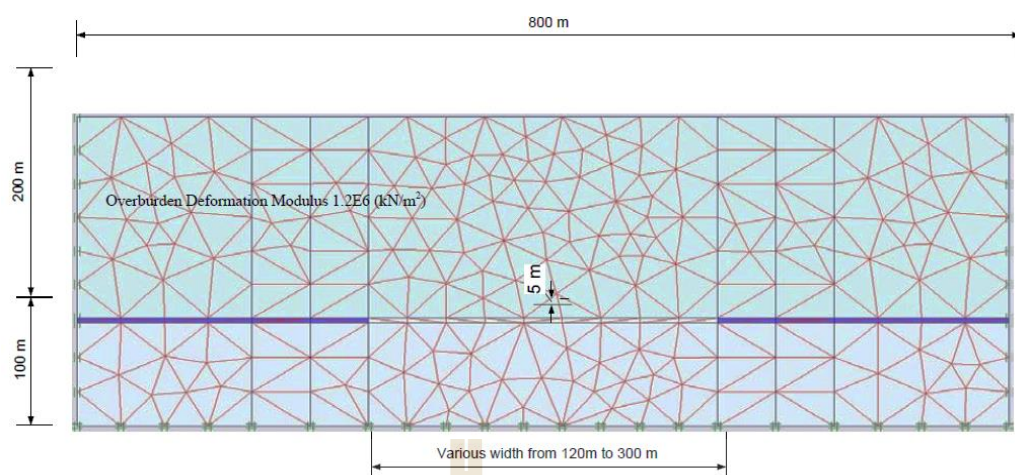
Figure 2.16 Basic subsidence mesh and model dimensions (Ren and Li, 2008).

Li and Zhu (2007) conclude that under various factors of affecting ground movement can be widely considered by the numerical method, which could predict ground movement caused by the underground excavation accurately. Numerical methods can deal with various rock and soil properties, complex boundary condition and time dependency. Auto generation of mesh is one of useful features of the numerical modelling software and another attractive feature.

Franzius et al. (2005) study both of 3D and 2D FEM of tunnel development in London Clay. The isotropic and anisotropic nonlinear models were performed, and it indicate that, a high degree of soil anisotropy, the transverse subsidence trough remains too shallow. Comparison of longitudinal subsidence profiles obtained from 3D analyses with data from field, it was illustrated that the horizontal trough enlarges too far in the horizontal direction.

2.5 Effect of underground opening and pillar geometries on surface subsidence

The pillar geometry can control its failure modes (Poulsen et al., Mark, 2006). Hill (2005) and Mark (2006) conclude that a pillar database in Australia and South Africa, found that most collapsed of pillars have a low width-to-height ratio (W/H). The W/H ratio less than 3 or 4 (slender pillars) may lead to a massive or sudden collapsed. For the W/H ratio between 4 and 8 (intermediate pillars), the failure form to be "squeeze", and W/H ratio exceeding 10 (squat pillars), the failure may start from the opening roof or floor. From the data can explain that the load condition of slender coal pillar is more reasonable to be in a uni-axial state than a tri-axial state caused the horizontal stress to pillar core is lacked. In addition, the pillar strength and the failure mode are affected by the pillar geometry or shape (Yu et al., 2017). Other factors may affect the stability of underground mining include temperature, in-situ stress and artificial disturbance. The rock strength and the rock burst probability will increase with high in-situ stress (Zhou, 2006).

Sartkaew and Fuenkajorn (2016) perform physical models to verify the accuracy of the hyperbolic, trigonometric and exponential profile functions that have been universally used to determine the surface subsidence under sub-critical to critical conditions induced by salt and potash underground mining. The physical models are using synthetic gel mixed with paraffin to demonstrate the overburden. A trap door apparatus is used to demonstrate the surface movement and to evaluate the effects of the opening geometry and mining depth. Figure 2.17 illustrates the trap door apparatus for physical simulation. The opening widths (W) are varied from 100 mm to 250 mm. The overburden thickness (Z) is varied from 40 to 100 mm. The opening height and length

are 10 and 200 mm. The results show that the angle of draw increases with increasing opening width. The maximum subsidence magnitude increases rapidly when the opening comes to be wider for each depth. The angle of draw more sensitive to opening width than depth. Application of the hyperbolic function would be conservative method for prediction the surface subsidence magnitude and slope for sub-critical to critical conditions.
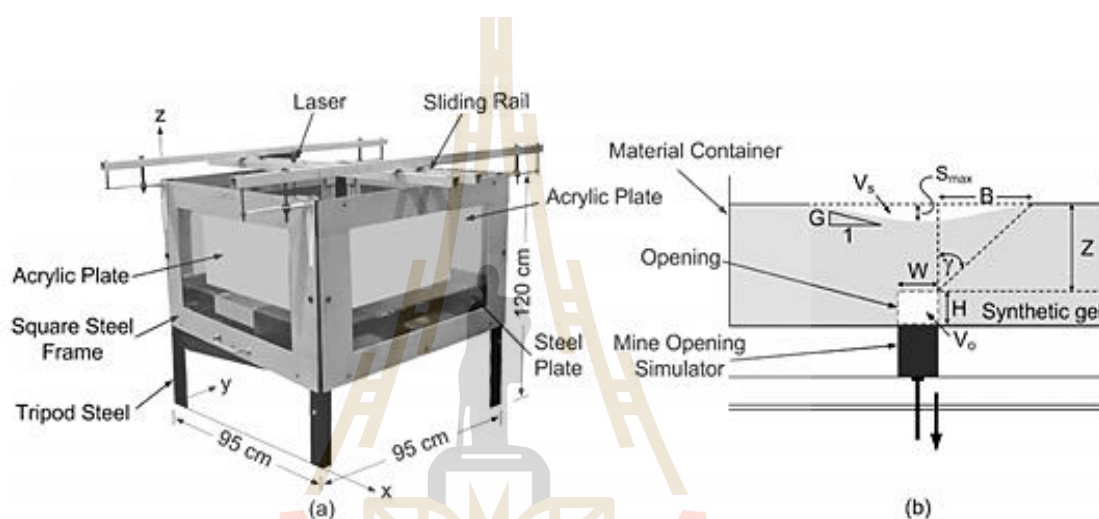
Figure 2.17 (a) Trap door apparatus for physical model test (b) Mine opening is simulated by plastic blocks (Sartkaew and Fuenkajorn, 2016).

Thongprapha et al. (2015) use the physical models to study the effects of the opening configurations on surface displacement under super-critical conditions. A trap door apparatus has been performed to the scaled-down simulations of ground subsidence and the opening width (W) is maintained constant at 5 cm. Clean gravel is applied to simulate the strata for demonstrate cohesionless behavior. The effects of opening height (H) and length (L) are evaluated by simulating the H/W varied from 0.2to 1 by incremental of 0.2, and L/W varied from 1, 2, 3, 4 to 5. The effects of opening depth or thickness (Z) is determined by varied Z/W from 1 to 3 to 4. The test

results show that the maximum subsidence, angle of draw, and volume of trough are controlled by the opening configurations (e.g. width, length, height and depth). The maximum surface subsidence and the angle of draw increase with increasing L/W ratios and when L/W equals 3, the maximum subsidence and angle of draw tend to approach a limit. In case of the same H/W ratio and L/W ratio, increasing the Z/W ratio decreases the maximum subsidence and angle of draw. The volume of ground surface subsidence trough obtained from the physical test is usually less than the opening closure volume (Figure 2.18). This cause from surface subsidence in the physical model has built new voids over the opening. However, the surface subsidence trough volume tends to reduce as the increasing of opening depth, particularly for short opening.
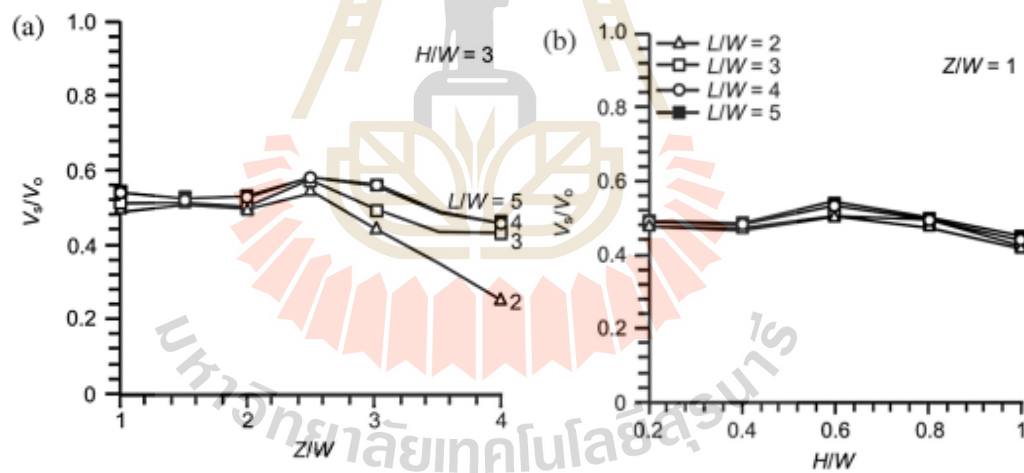
Figure 2.18 Surface trough volume-to-opening volume (V_s/V_o) as a function of mining depth ratio Z/W (a) and mining height ratio H/W (b) four values of L/W ratios (Thongprapha et al., 2015).

CHAPTER III

PHYSICAL MODEL TESTS

3.1   Introduction

The objective of physical model simulations in this study is to assess the effects of pillar geometries on surface subsidence under sub-critical condition. This section describes method, apparatus and test result data of the simulations.

3.2   Design and fabrication of test apparatus

The functional requirements for the test frame are (1) to simulate surface subsidence of strata in three-dimension, (2) to estimate the effect of the underground opening geometries on surface subsidence, and (3) to induce subsidence of overburden under true gravitational force.

The trap door apparatus (Thongprapha et al., 2015) consists of three main components: the material container, the underground opening simulator, and the ground surface measurement system. A custom-made of 90.6×40 cm^2 clear acrylic plate (thick 10 mm) is placed in the trenches of the steel frame. Four acrylic sheets are secured with a steel plate at each side. The space of testing is 88.6×38×20 cm^3. The mine opening simulator is a plastic blocks array of 86 mm wide, 380 mm long and 10 mm high, when the length of the opening is beyond 3 times of the opening width, the angle of draw tends to approach a limit (Thongprapha et al., 2015). The blocks are used to simulate the underground openings by first placing them below the material container. After the

synthetic gel set with predefined overburden thickness, the blocks are systematically

moved down to simulate the opening, and hence the surface subsidence occurs.

The measurement system comprises of a laser scanner on sliding rail. The laser

scanner can be moved in two directions. The measurements precision is one micron.

The surface subsidence profile is recorded and plotted in three-dimension. The

maximum surface subsidence values, angles of draw and subsidence extent can be

determined for each opening geometry. Figures 3.3 through 3.7 illustrate the schematic

drawings of the test apparatus.
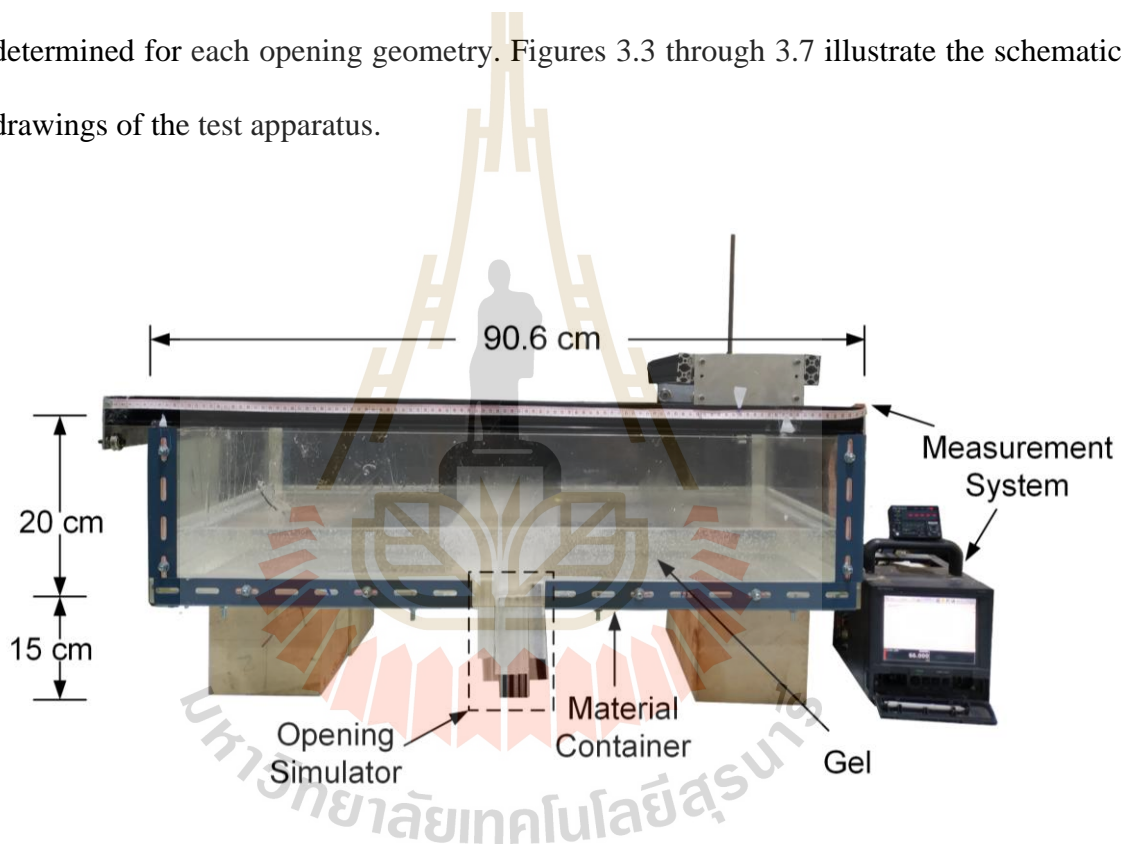
Figure 3.1 Trap door apparatus used for physical testing.
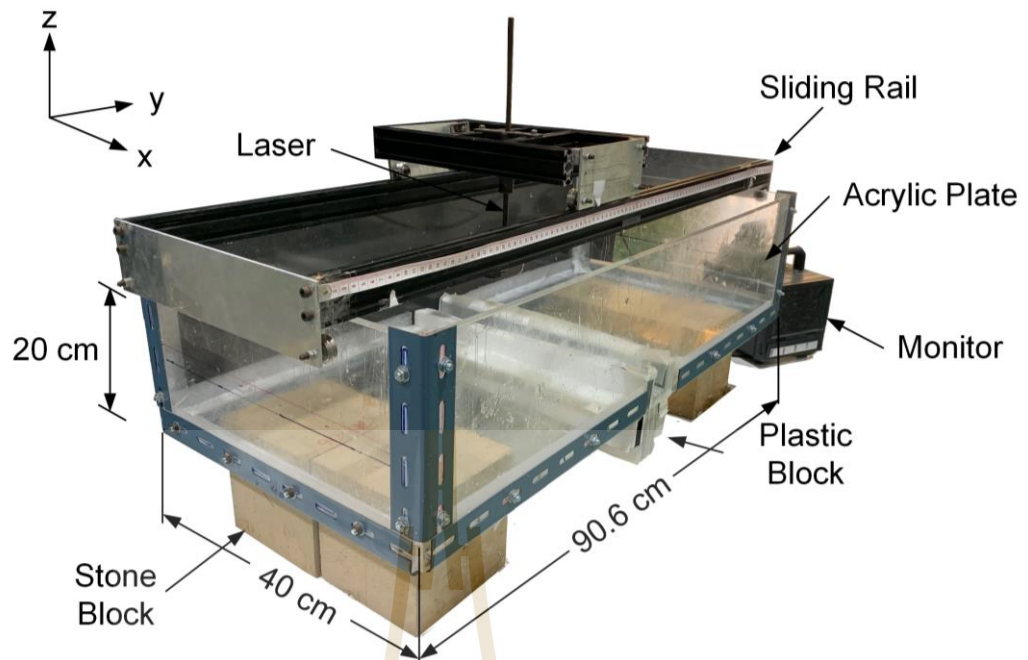
Figure 3.2 Trap door apparatus used for physical testing.
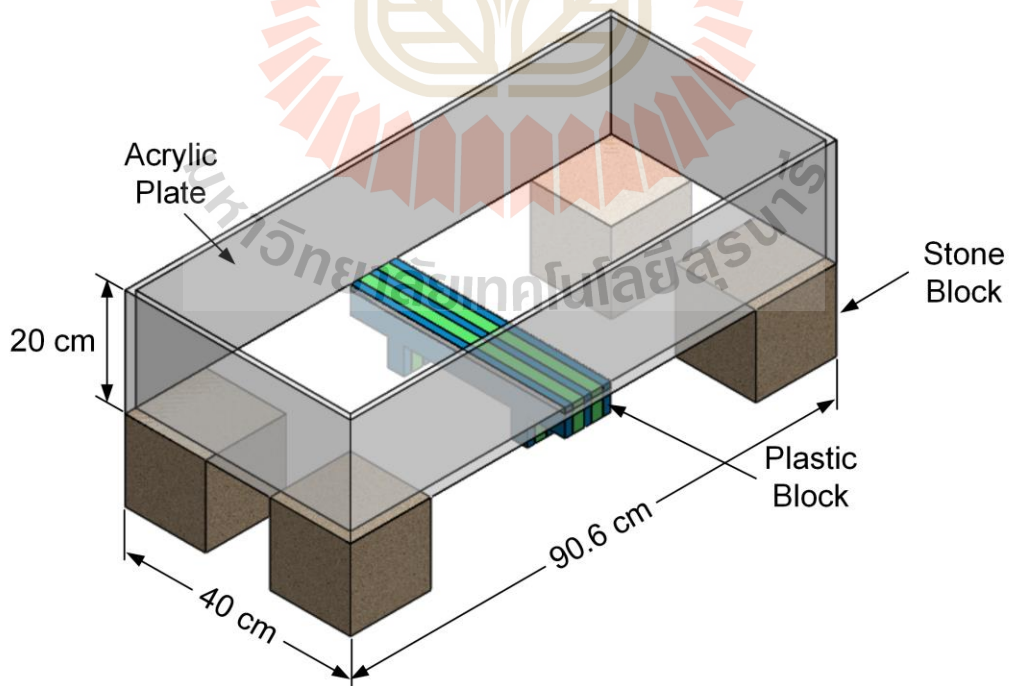
Figure 3.3 Perspective view of trap door apparatus.
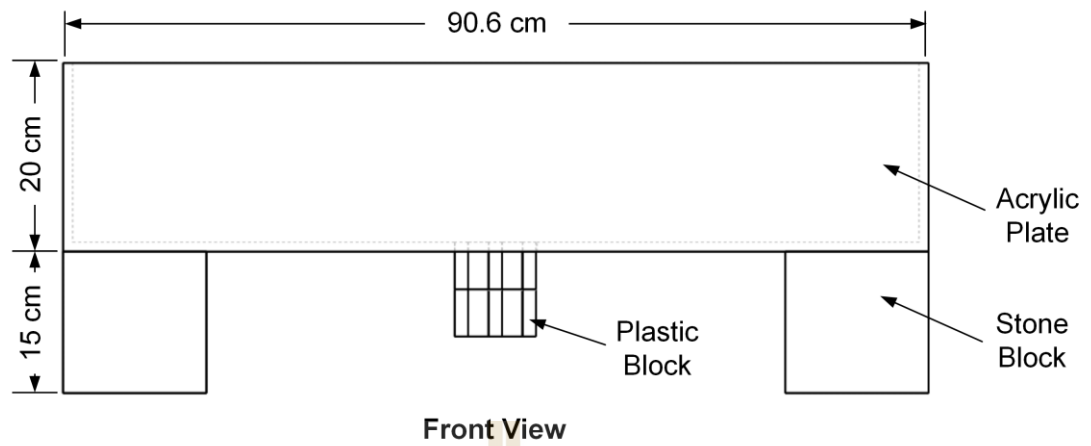
Figure 3.4 Front view of trap door apparatus.
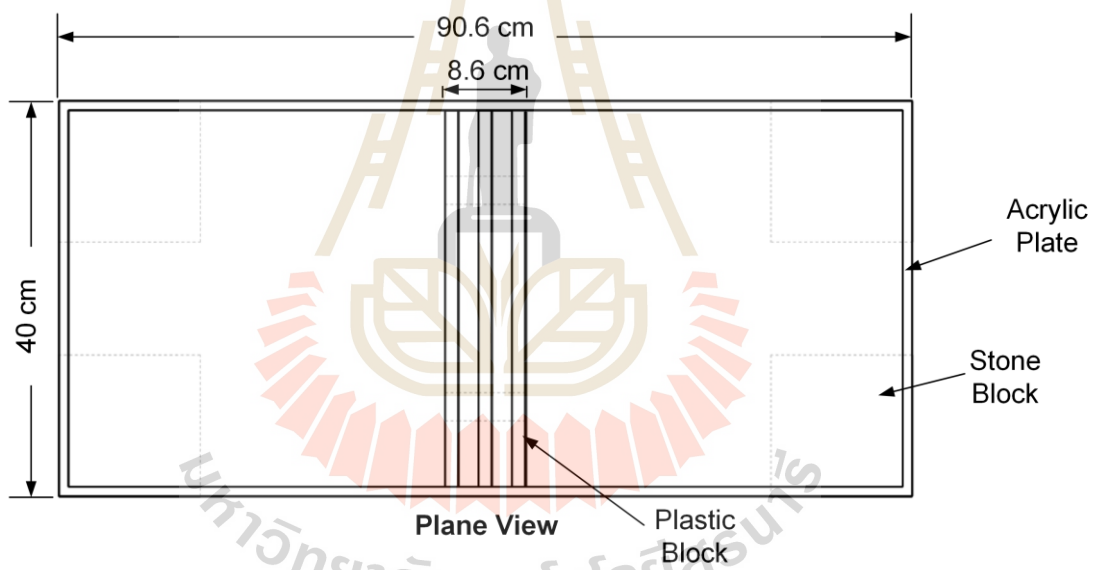
Figure 3.5 Plane view of trap door apparatus.
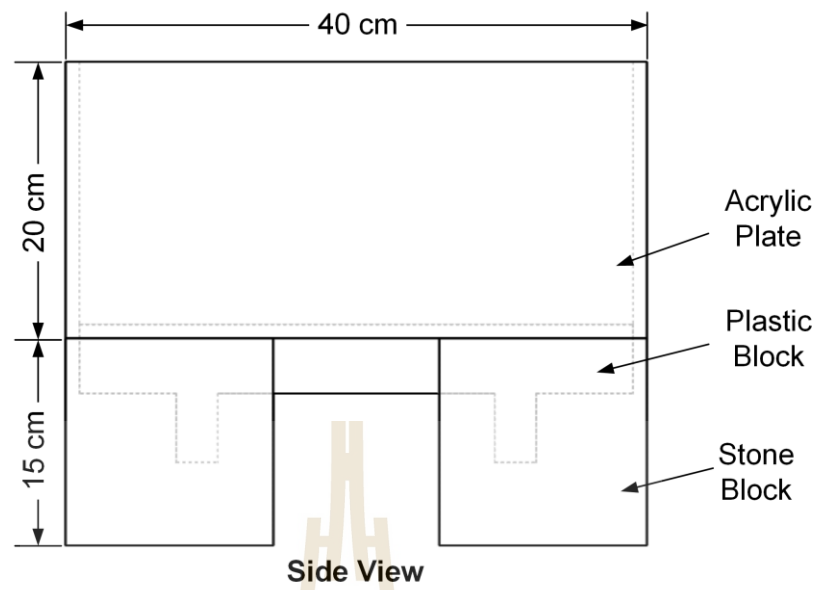
Figure 3.6 Side view of trap door apparatus.
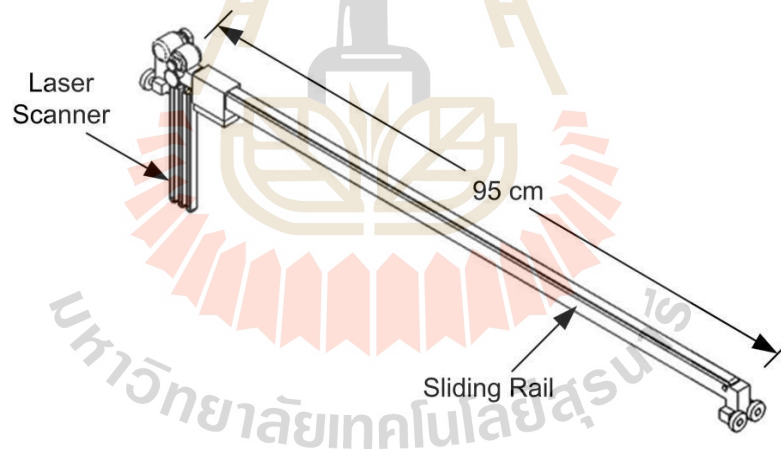
Figure 3.7 Measurement system of trap door apparatus.

3.3   Material preparation

The material used to simulate the overburden is universally obtainable and non-toxic. The synthetic gel (mineral oil, C_nH_{2n+2}) is selected here due to it is greatly uniform in terms of physical and mechanical properties. These properties tend to be stable with variations of temperature and humidity. The synthetic gel has been melted under the temperature of 100°c in the oven (Figure 3.8) and then it is poured into the PVC pipe of 17.5 mm diameter and 35.0 mm length to obtain cylindrical gel specimen with L/D ratio of 2.0. The gel becomes semi-solid material after curing time for 24 hours (Figure 3.9). The uniaxial compression test is conducted to determine the elastic modulus of the gel by using universal testing machine (UTM). The test method and calculation follow the ASTM D695-15 standard practice. Table 3.1 summarizes dimensions and physical properties of specimens. The average density of the gel specimens is about 0.92 ± 0.03 g/cm^3. Figures 3.11 show the stress-strain relation curves obtained from testing. The elastic modulus is calculated from stress-strain curves under cyclic loading and unloading. The elastic moduli and Poisson's ratios of the gel are summarized in Table 3.2. The elastic modulus of 8.31 kPa and Poisson's ratio of 0.36 are used to simulate the overburden properties.

Figure 3.8 Synthetic gel under 100°c.

Gel-UCS-01   Gel-UCS-02   Gel-UCS-03

0   10 mm
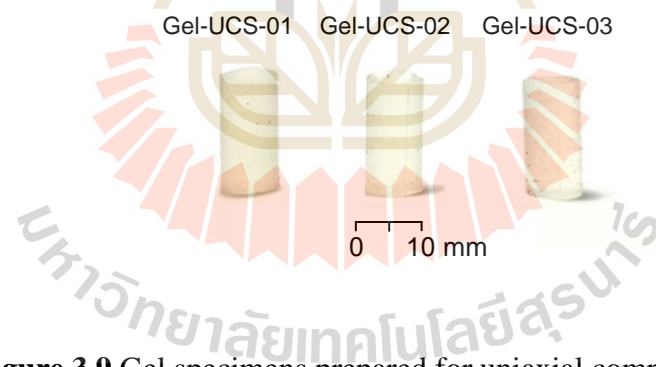
Figure 3.9 Gel specimens prepared for uniaxial compression test.

Table 3.1 Synthetic gel specimen dimensions prepared for uniaxial compression testing.

Specimen no.	Diameter (mm)	Height (mm)	Weight (g)	Volume (cm^3)	Density (g/cm^3)
Gel-UCS-01	16.90	35.60	7.31	7.99	0.92
Gel-UCS-02	17.10	35.90	7.40	8.25	0.90
Gel-UCS-03	16.58	34.00	6.99	7.34	0.95
Average ± SD					0.92 ± 0.03
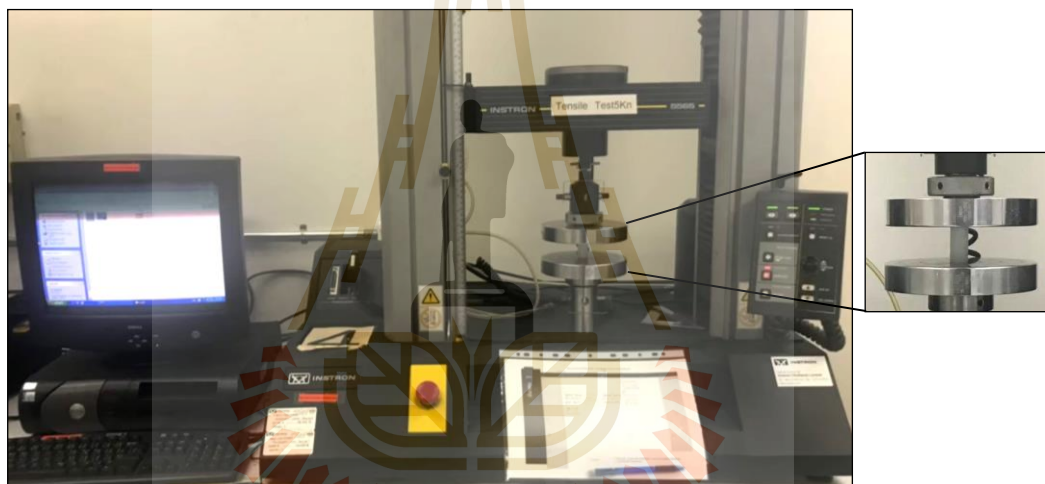
Figure 3.10 Gel specimen placed in universal testing machine (UTM).
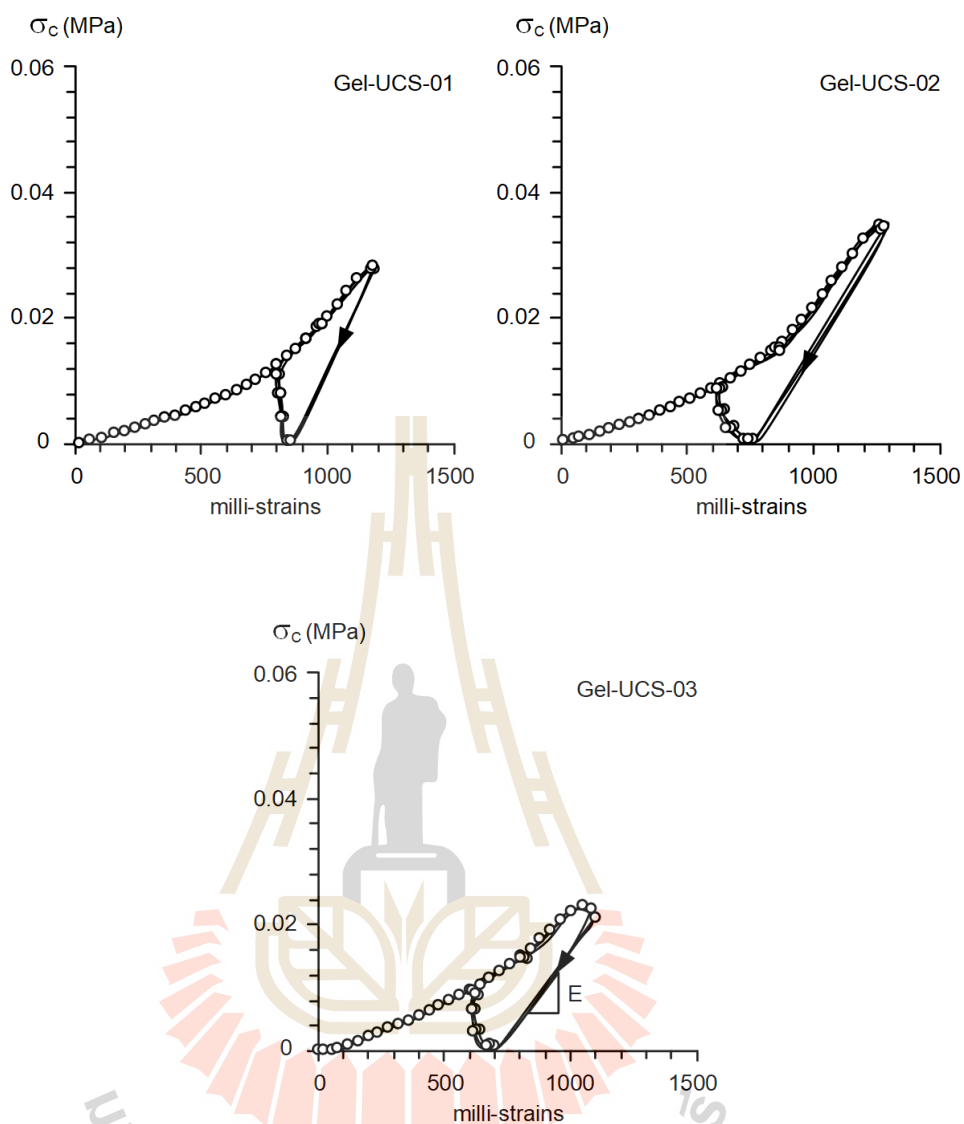
Figure 3.11 Stress-strain curves obtained from gel specimens.

Table 3.2 Mechanical properties of gel obtained from uniaxial compression testing.

Specimen no.	Elastic modulus (kPa)	Poisson's ratio
Gel-UCS-01	8.35	0.36
Gel-UCS-02	8.91	0.36
Gel-UCS-03	7.66	0.35
Average ± SD	8.31 ± 0.62	0.36 ± 0.01

3.4   Preliminary investigation

The preliminary investigations have been performed to estimate the effects of pillar geometries on surface settlement under sub-critical condition. The subsidence components considered here include maximum surface subsidence (S_{max}), angle of draw (γ) and subsidence extent (B). SolidWorks used to simulate three cases of different pillar geometries under constant area extraction ratio at 50%, as shown in Figure 3.12, the area extraction ratio (e_a) can be calculated as follows:

$$e_a\,(\%) = \frac{\text{extraction area}}{\text{total area}} \times 100\% \tag{3.1}$$

The mine area width (W_m) and mine height (H) is maintained constant at 86l mm and 20 mm and mine length (L) is 380 mm. The overburden thickness (D) or opening depth is 100 mm. For each cases of simulations, the overburden used the synthetic gel properties (Table 3.1 and Table 3.2). Figure 3.13 shows example of boundary conditions and mesh models of case C. The results are recorded and plotted in two-dimensional profiles. The subsidence profiles are used to determine the surface subsidence components, including the maximum subsidence, angle of draw and subsidence extent, where S_{max} is measured above the middle of the opening, γ is the angle between a vertical line from the edge of the underground opening and a line from the edge of the limit of surface subsidence to the point at 1% of the S_{max} and B is width limit of the surface subsidence trough. The subsidence profile in Figure 3.14 indicates that the maximum subsidence, angle of draw and surface subsidence extent are relatively equal in all cases. The results are shown in Table 3.3. The subsidence components tend to be independent of pillar geometries under the same extraction ratio.
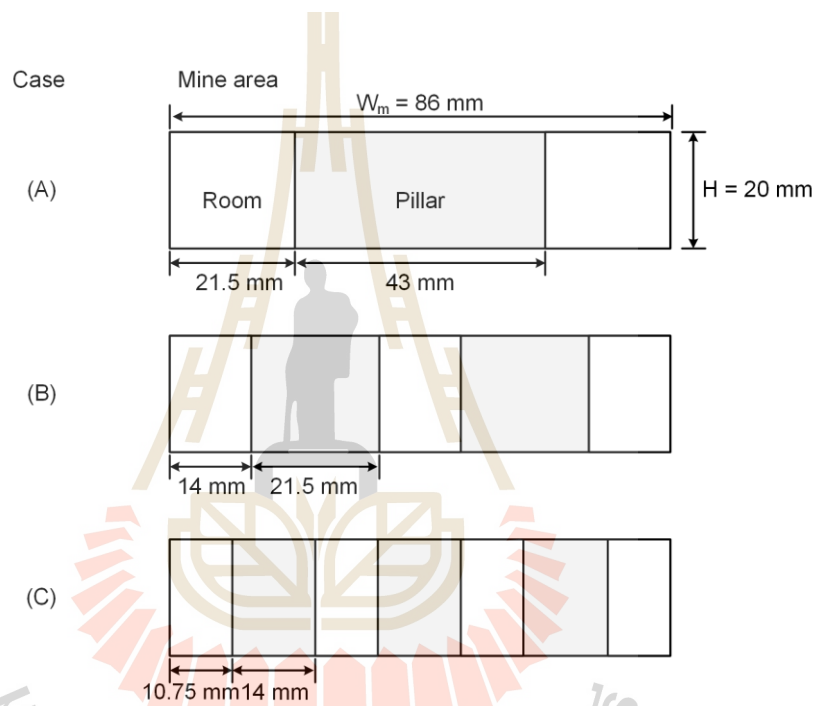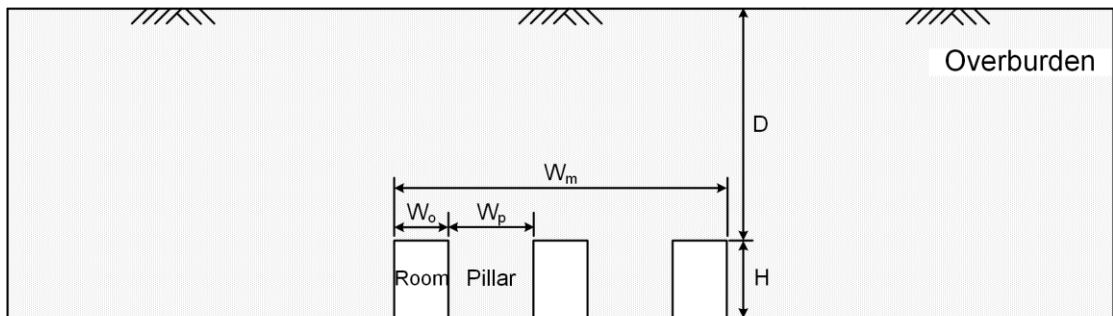
Figure 3.12 Mining configurations simulated in the physical models.
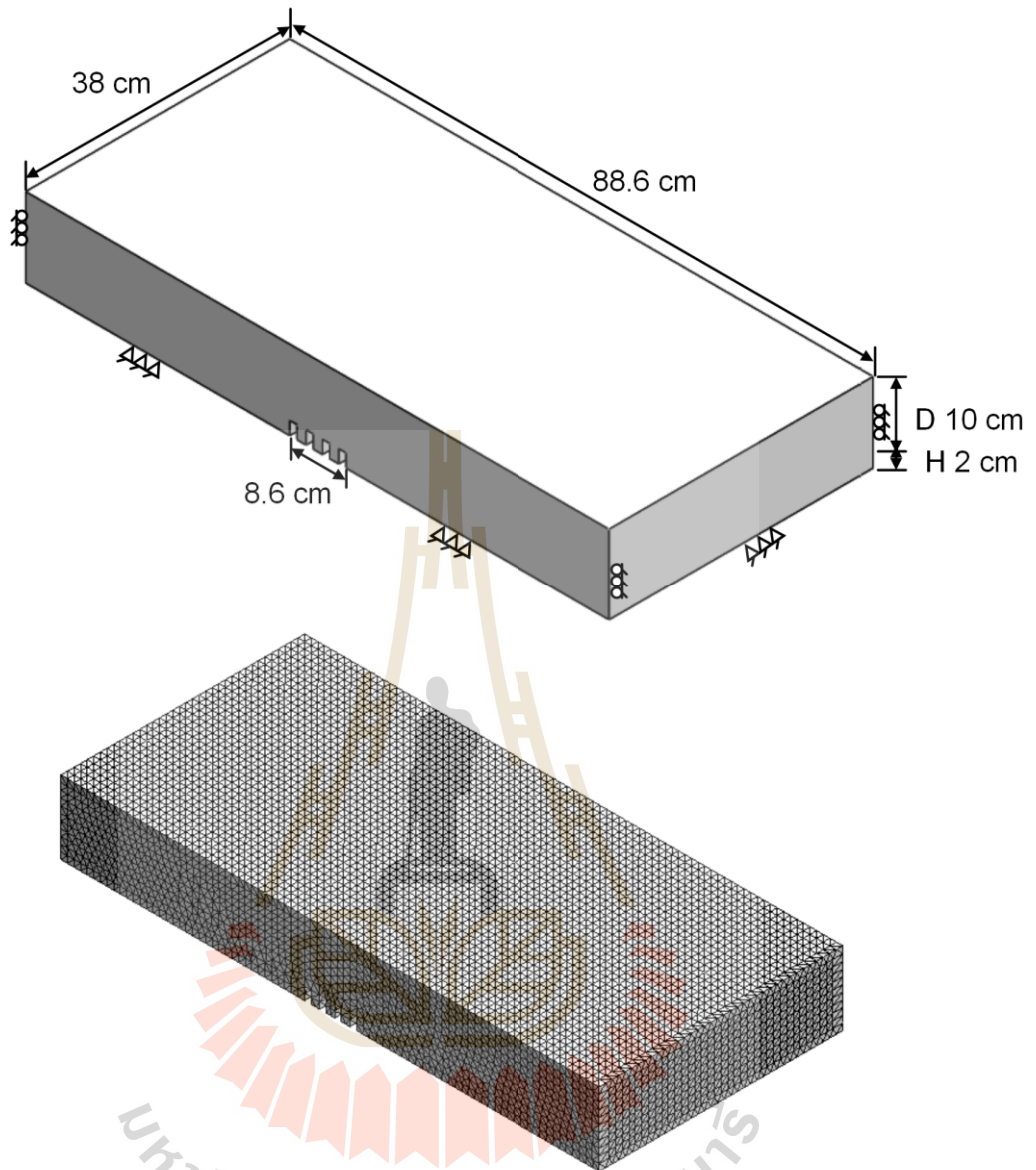
Figure 3.13 Boundary conditions and mesh models of case C.
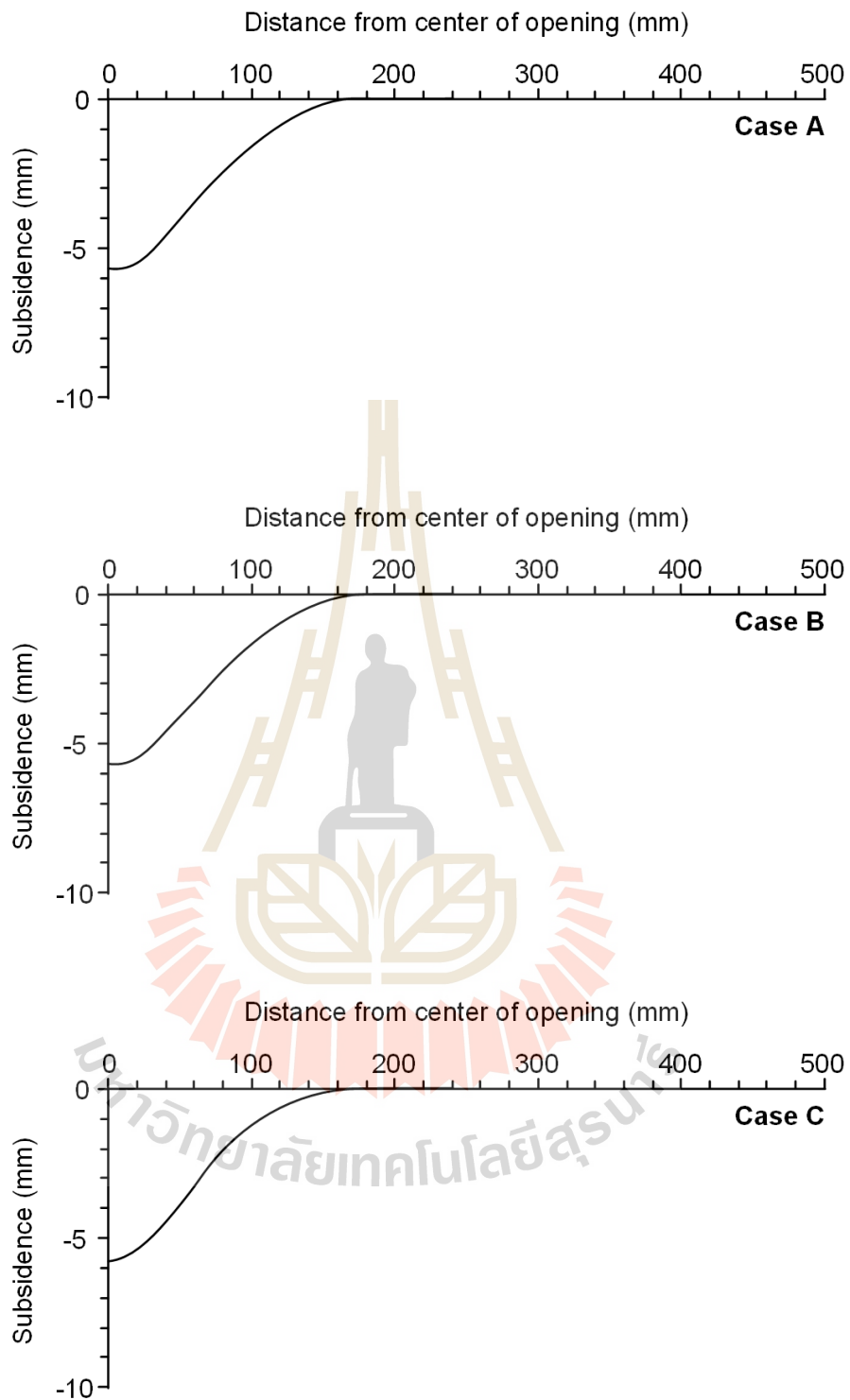
Figure 3.14 Subsidence profile for different opening widths. Vertical scale is exaggerated.

Table 3.3 Preliminary model results with constant extraction ratio of 50%.

Case	W_o (mm)	H (mm)	S_{max} (mm)	B (mm)	γ (degrees)
A	21.50	20	5.776	133	53.1
B	14.00	20	5.766	136	53.7
C	10.75	20	5.768	138	54.1

3.5 Physical model testing

The physical simulations have been performed to verify the preliminary investigation of sub-critical surface subsidence. A trap door apparatus used to illustrate the scaled-down three-dimensional simulations of surface settlement which allows completely controlled test conditions. Three cases of different pillar geometries as section 3.4 are simulated under constant area extraction ratio at 50% (Figure 3.12). For each cases of simulations, the synthetic gel is melted to obtain viscous fluid under the temperature of 100°c. It is poured in the container to a predefined thickness (Figure 3.15), pour the gel while it is still hot and slowly pour into the container along the side, to reduce the chance of bubbles. The synthetic gel layer thickness represents the opening depth or the overburden thickness. After the synthetic gel becomes semi-solid form under ambient temperature for 24 hours, the blocks are gradually and systematically moved down, and induces the vertical displacement of the synthetic gel above occurs. The laser scanner is used to measure the surface subsidence profile of the overburden before and after the subsidence is induced. The results are recorded and plotted in two-dimensional profiles. The subsidence profiles are used to determine the subsidence components, including the maximum subsidence, angle of draw and subsidence trough width.
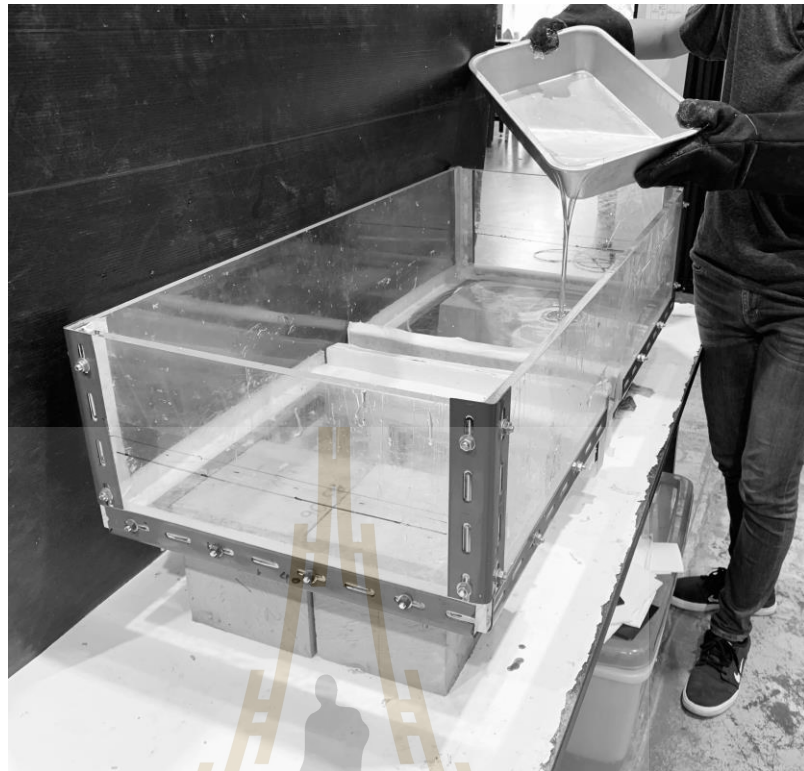
Figure 3.15 Filling synthetic gel into material container.
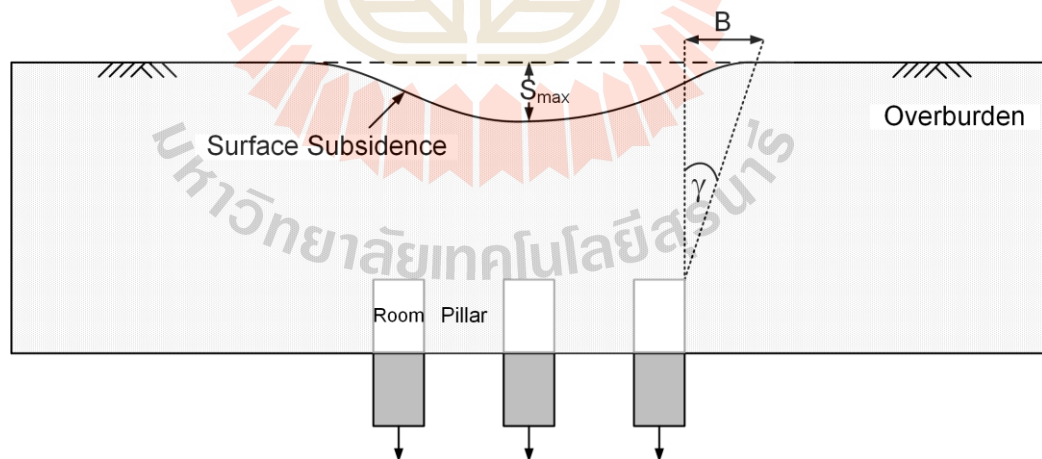
Figure 3.16 Trap door apparatus used in the physical simulations.

Figure 3.17 shows the example of a scanned three-dimensional image and its cross section. The subsidence profile in Figure 3.18 indicates that the maximum subsidence, angle of draw and surface subsidence extent are relatively equal in all

cases. The results are shown in Table 3.4. The physical model results agree well with those results obtained from preliminary investigation. The subsidence components tend to be independent of pillar geometries under the same extraction ratio. This is because the subsidence depends only on mine extracted volume. However, preliminary investigation and physical model testing are simplified (two-dimensional problem), the effect of pillar geometries in complex condition (three-dimensional problem) is needed.
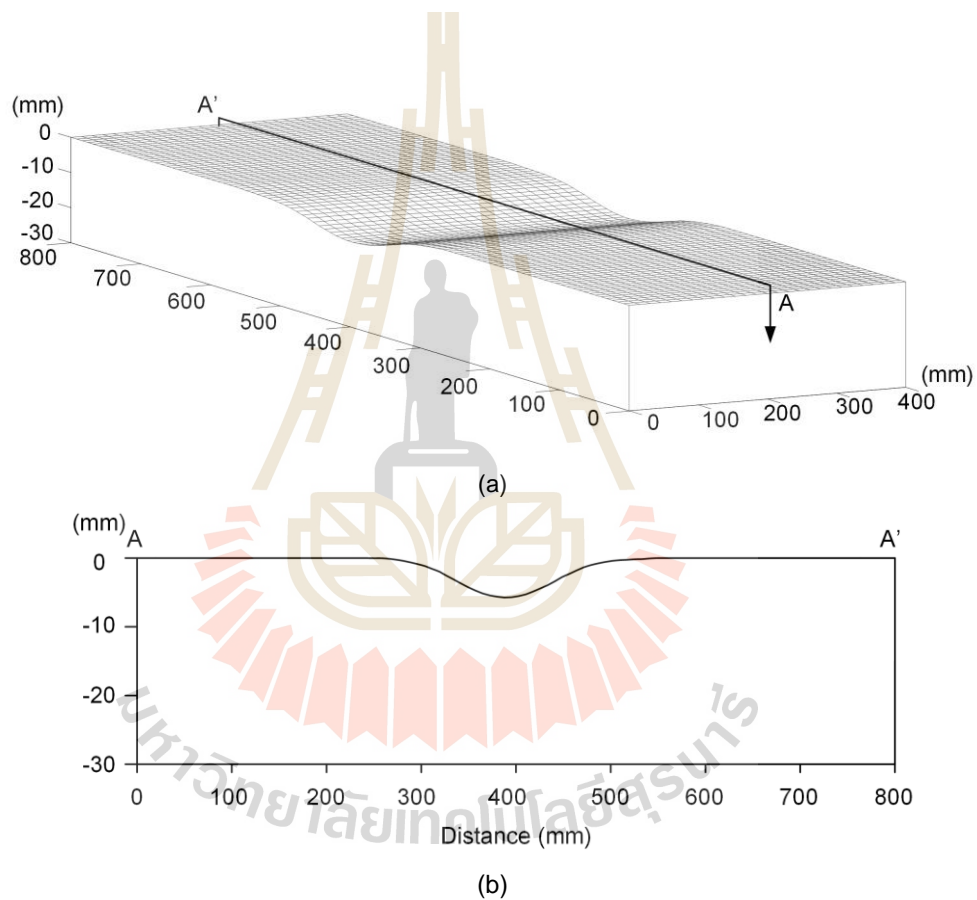
Figure 3.17 Example of three-dimensional image of gel subsidence for model case B (a) and cross-section (b). Vertical scale is greatly exaggerated.
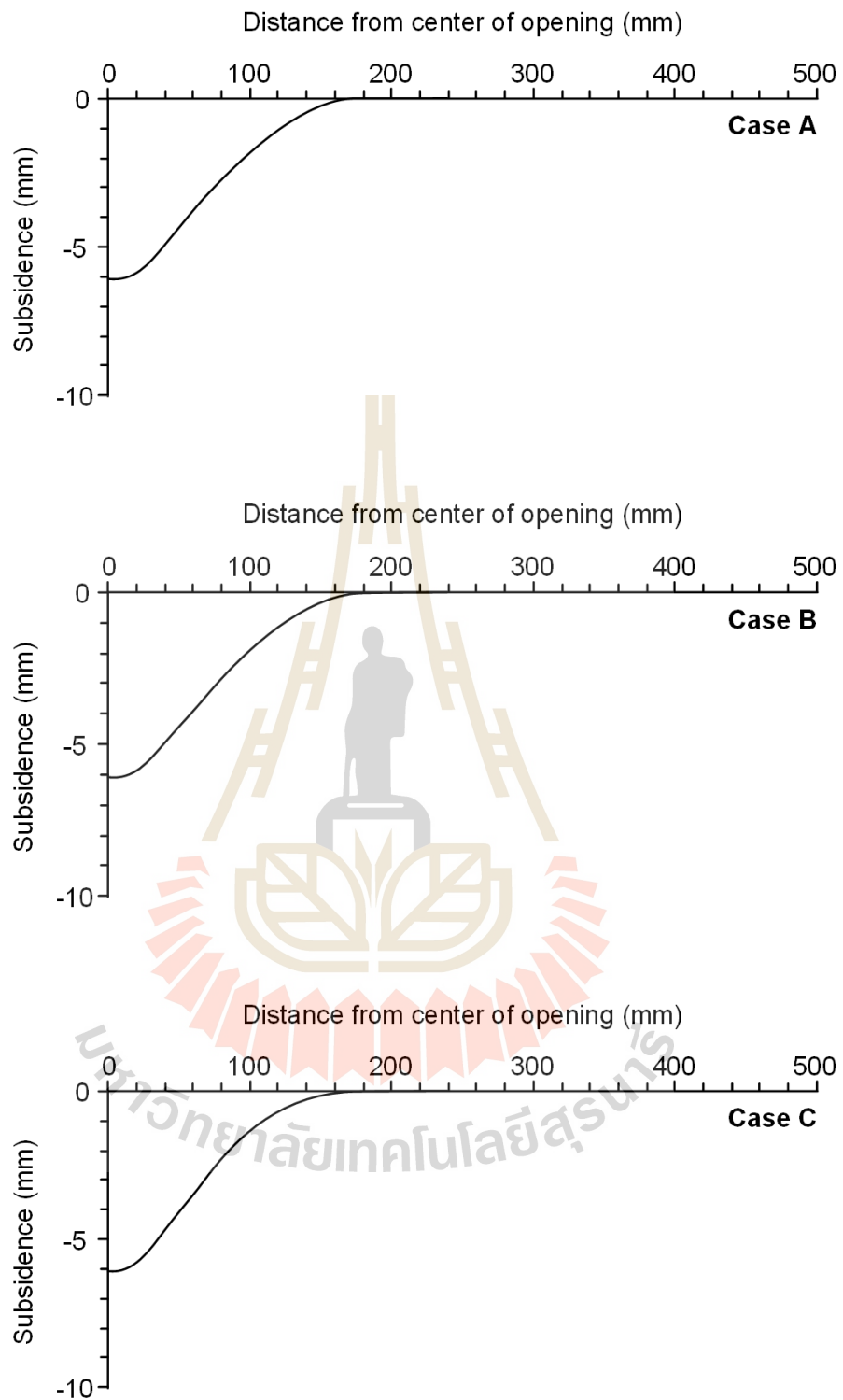
Figure 3.18 Line scanned profile of surface subsidence for different opening

configurations. Vertical scale is exaggerated.

Table 3.4 Physical model test results with constant extraction ratio of 50%.

Case	W_o (mm)	H (mm)	S_{max} (mm)	B (mm)	γ (degrees)
A	21.50	20	6.121	142	54.8
B	14.00	20	6.104	147	55.7
C	10.75	20	6.136	148	55.9

CHAPTER IV

NUMERICAL SIMULATIONS

4.1   Introduction

This section describes the results of finite element analyses using SolidWorks (Dassault Systemes, 2017). The objective of numerical simulations is to determine the effects of mine panel geometries and overburden properties on surface subsidence. SolidWorks is used to determine the surface subsidence under various pillar shapes, opening heights, mine depths, abutment pillar widths, and elastic moduli.

4.2   Three-dimensional simulations

SolidWorks is used to simulate the ground subsidence. It has been used here because it allows creating various mine panel geometries under three-dimensions. To avoid complex and non-uniformity of rock strata in the field, the overburden properties are assumed. The elastic modulus (E) is defined as 10 GPa, density is 2,700 kg/m^3 and Poisson's ratio (v) is 0.25 for all cases. The strength properties of rock are not considered here because the opening and ground surface are not allowed to fail. The test variables include pillar geometries in terms of pillar width in x-axis-to-pillar width in y-axis ratio (W_x/W_y), pillar heights (H), mining depths (D), elastic moduli (E), and abutment pillar widths (W_{ab}), as shown in Table 4.1.

Table 4.1 The parameters used in SolidWorks simulations.

Series	Variable parameters		Constant parameters
I	Pillar shape (W_x/W_y)	0.25	H = 6 m, D = 200 m, E = 10 GPa
		0.50	
		0.75	
		1.00	
		1.25	
		2.70	
II	Pillar height (H)	2 m	W_x/W_y = 1.00, D = 200 m, E = 10 GPa
		4 m	
		6 m	
		8 m	
		10 m	
III	Opening depth (D)	100 m	W_x/W_y = 1.00, H = 6 m, E = 10 GPa
		150 m	
		200 m	
		250 m	
		300 m	
IV	Elastic modulus (E)	5 GPa	W_x/W_y = 1.00, H = 6 m, D = 200 m
		10 GPa	
		20 GPa	
		30 GPa	
V	Abutment pillar width (W_{ab})	25 m	W_x/W_y = 1.00, H = 6 m, D = 200 m, E = 10 GPa
		50 m	
		75 m	
		100 m	

All test series are simulated under different volumetric extraction ratios (e_v) of 40, 50 and 60%. The volumetric extraction ratio (e_v) can be calculated as follows:

$$e_v\,(\%) = \frac{\text{extraction volume}}{\text{total volume}} \times 100\% \tag{4.1}$$

The results are presented in terms of the maximum surface subsidence-to-mine depth ratio (S_{max}/D), angle of draw (γ), and subsidence trough width-to-panel width ratio (B/W). The S_{max} is measured above the center of the opening, γ is the angle between a vertical line from the edge of the underground opening and a line from the edge of the limit of surface subsidence to the point at 1% of the S_{max}, and B is width limit of the surface subsidence trough, as shown in Figure 4.1.
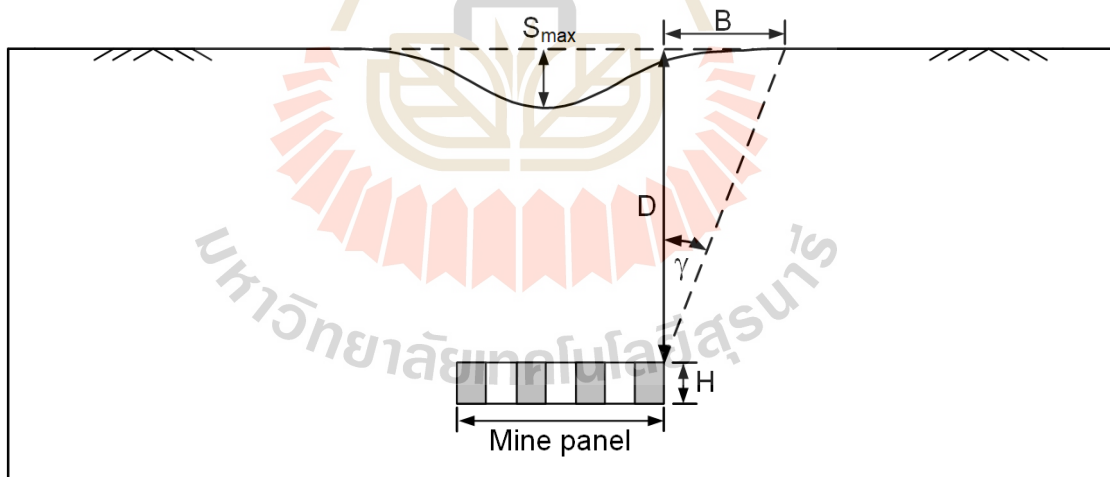
Figure 4.1 Surface subsidence components.

4.2.1 Boundary conditions

The block models are symmetries in x and y axes. A quarter of the modelling is needed for the simulations. The width and length of rectangular boundaries are 500 m, and the height is 215 m (Figure 4.2). The lateral boundaries are fixed in the horizontal direction and the bottom boundary is fixed in the vertical direction.

The upper surface boundary can move freely in both directions. The rectangular panel located at the center of boundary is maintained constant at 50 m width and 100 m length for all cases. The overburden above the opening is 200 m. The distance between the opening floor and the bottom boundary is 15 m. For cover the entire range of the underground opening dimensions, over 150,000 tetrahedral elements have been performed to obtain correct simulation results. The very fine mesh with element size of 2.5 m^2 is prepared around the underground opening due to the stress and strain gradients are high in this area (Figure 4.3). The mesh far from the opening is gradually coarser. To simulate the underground opening, the meshes inside the opening boundary are deleted. Initial stress due to gravitational loading is calculated from density of the overburden. The data iteration of about 100,000 cycles are performed.
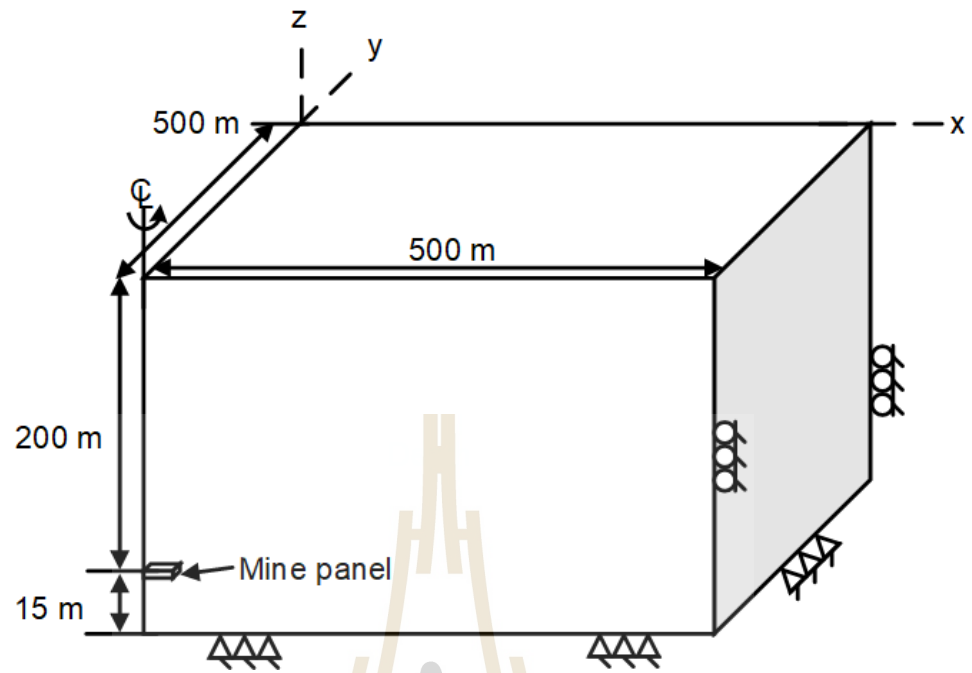
Figure 4.2 Quarter of boundary conditions for SolidWorks simulations.
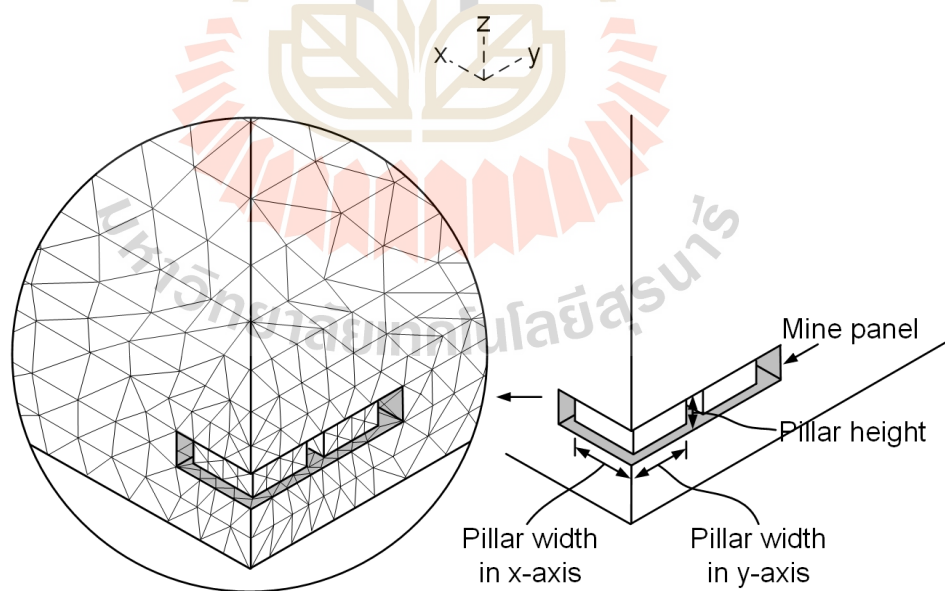
Figure 4.3 Mesh model for SolidWorks simulations.

4.4.2 Effect of pillar geometries

The pillar geometries (W_x/W_y) are varied from 0.25 to 2.70 (Figure 4.4 and Table 4.2). The opening depth and height are constant at 200 m and 6 m, respectively. The elastic modulus and Poisson's ratio of the overburden are 10 GPa and 0.25. Figure 4.5 illustrates an example of surface subsidence obtained from computer simulations and its cross-section. Figure 4.6 shows the normalized maximum subsidence (S_{max}/D), trough width (B/W) and angle of draw (γ) for varied pillar geometries and extraction ratios, as a function of pillar width in x axis-to-pillar width in y axis ratios (W_x/W_y). The results indicate that the S_{max}/D and B/W ratios tend to be independent of pillar shapes (W_x/W_y). The S_{max} is however sensitive to extraction ratios. This is because mine subsidence depends only on mining extracted volume. The γ and B are not sensitive to the extraction ratio. This is probably due to that the γ depends on stiffness of overburden strata (Ren and Li, 2008, Sartkaew et al., 2018,).
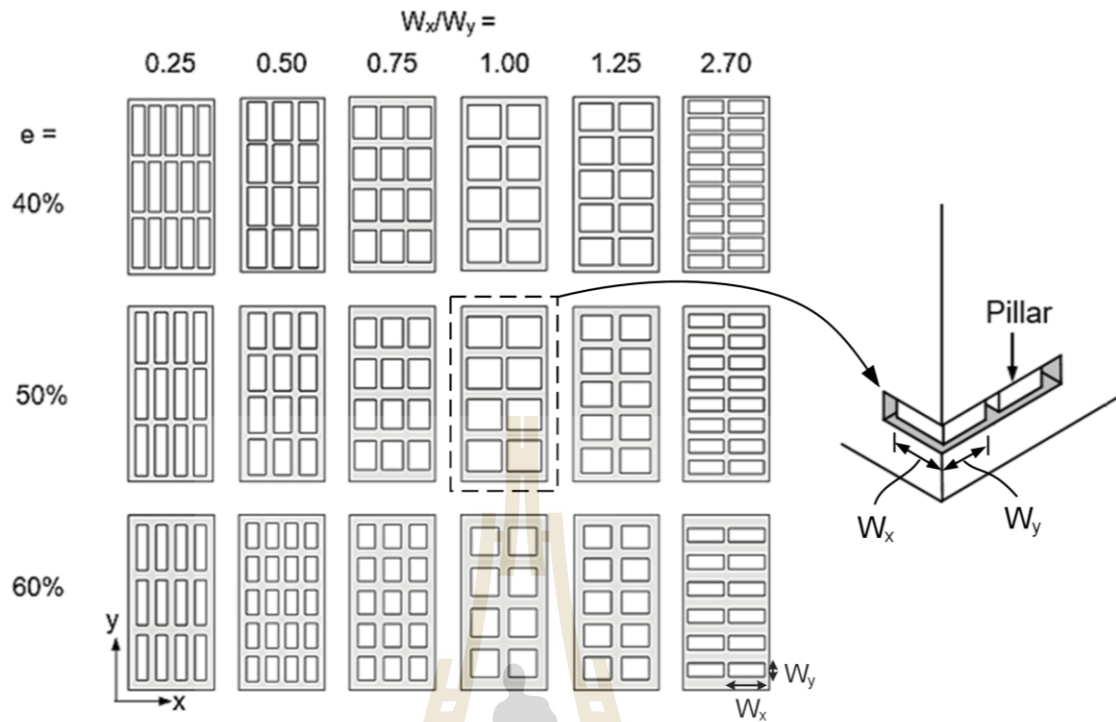
Figure 4.4 Plan view of mine panel geometries used in simulations.

Table 4.2 Pillar dimensions in mine panel.

e (%)	W_x/W_y ratios											
	0.25		0.50		0.75		1.00		1.25		2.70	
	W_x (m)	W_y (m)	W_x (m)	W_y (m)	W_x (m)	W_y (m)	W_x (m)	W_y (m)	W_x (m)	W_y (m)	W_x (m)	W_y (m)
40	7.1	28.4	11.2	22.3	13.7	18.2	19.3	19.3	19.5	15.6	20.2	7.5
50	7.2	28.8	10.2	20.4	12.4	16.5	17.7	17.7	17.7	14.1	20.4	7.6
60	6.5	25.8	7.1	14.1	10.0	13.3	16.0	16.0	16.0	12.8	21.0	7.8

(a)

Distance (m)

(b)
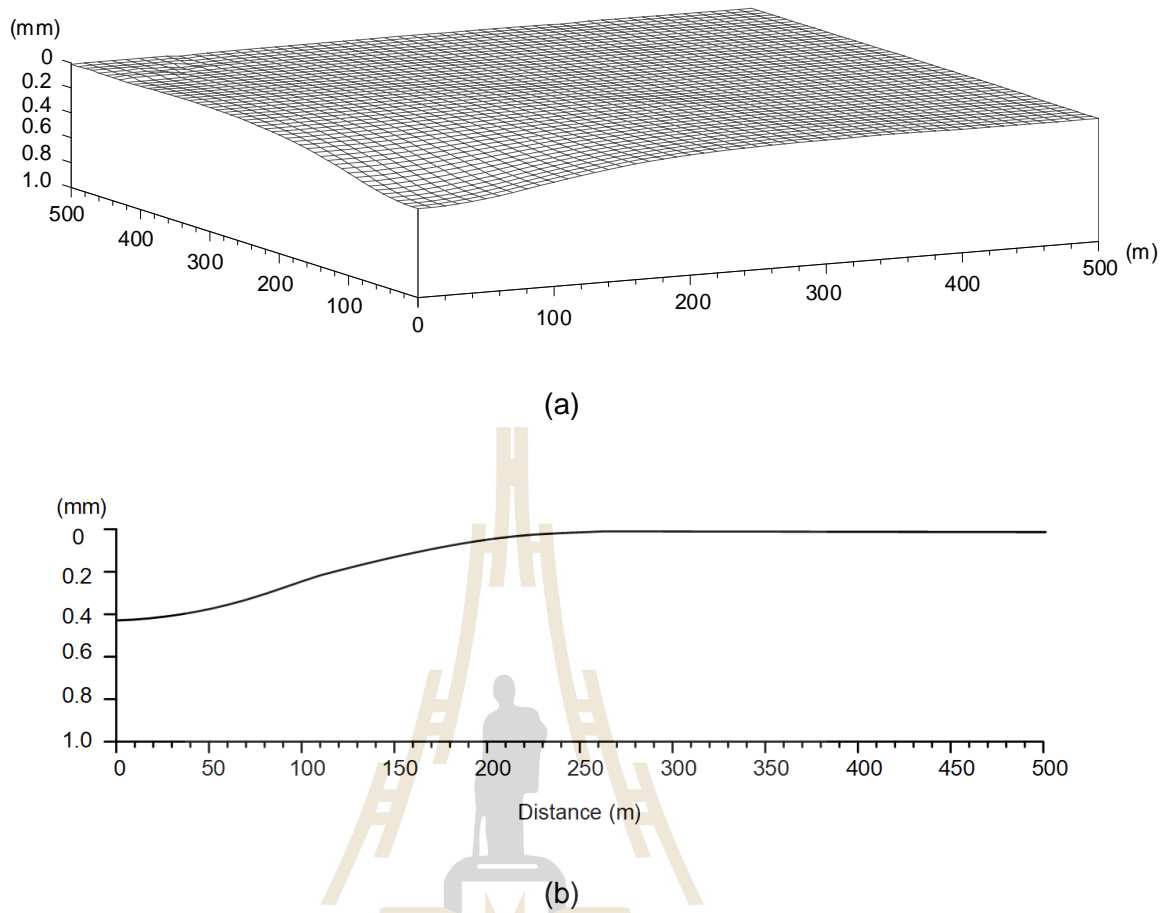
Figure 4.5 Example of 3D simulations of ground subsidence for $W_x/W_y = 1.00$ (a) and

its cross-section (b). Vertical scale is greatly exaggerated.
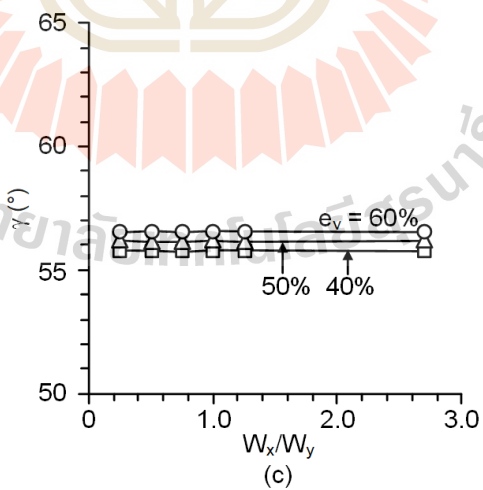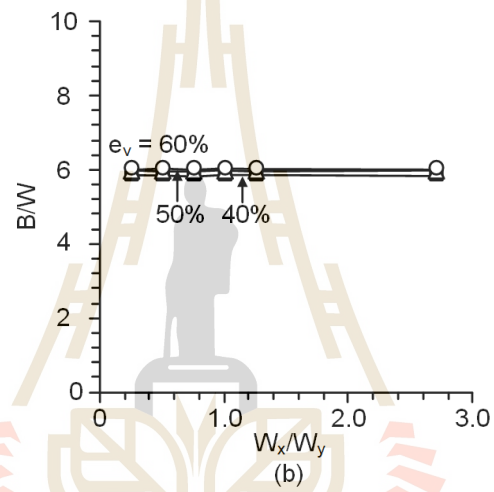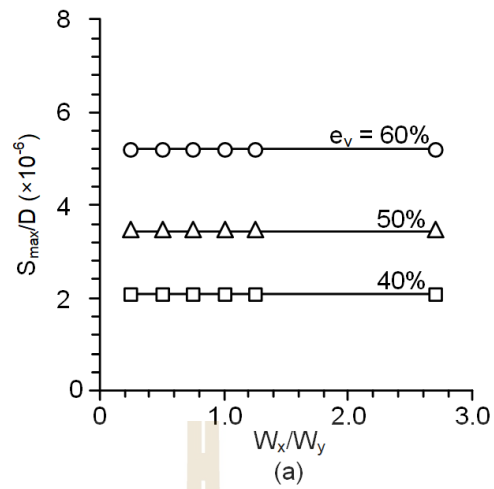
Figure 4.6 (a) Normalized maximum subsidence (S_{max}/D), (b) normalized subsidence

extent (B/W) and (c) angle of draw (γ) as a function of W_x/W_y ratios for

mine depth of 200 m.

4.2.3 Effect of pillar height

The opening height varies from 2, 4, 6, 8 to 10 m. The opening depth is constant at 200 m. The W_x/W_y ratio for all simulations is 1.00. The elastic modulus of the overburden is 10 GPa and Poisson's ratio is 0.25. Figure 4.7 shows the subsidence component results for varied pillar heights and extraction ratios, as a function of pillar height-to-depth ratios (H/D). The results indicate that the S_{max}/D ratios, γ and B/W ratios increase gradually with increasing H/D ratios and e. At the higher H/D ratios, the subsidence under each extraction ratio is widely divergent because the extraction volumes increase with increasing opening height, but γ and B is not sensitive to the extraction ratios. The results agree with Hustrulid (1976), Zipf (2001) and Thongprapha et al. (2015) who conclude that the pillar strengths increase with decreasing the pillar heights, and the angle of draw increases with increasing pillar heights. Furthermore, Yao et al. (1991) state that increasing the overburden strengths would reduce the angle of draw.

4.2.4 Effect of opening depth

The opening depths or overburden thickness are varied from 100, 150, 200, 250 to 300 m. The opening height is constant at 6 m. The W_x/W_y ratio for all simulations is 1.00. The elastic modulus of the overburden is 10 GPa and Poisson's ratio is 0.25. Figure 4.8 shows the subsidence components for varied depths and extraction ratios, as a function of opening depth (D). The results indicate that the S_{max}/D ratios and γ decrease with increasing mining depths, while B/W ratios increase with increasing mining depths. The γ and B/W ratios are not sensitive to the extraction ratio. This agrees well with the results obtained from Sartkaew et al. (2018) who performed

the physical model simulation and conclude that the increasing of the overburden thickness can reduce the maximum subsidence.

4.2.5 Effect of elastic modulus

The elastic moduli of overburden are assumed varying from 5, 10, 20 to 30 GPa. The opening depth and height are constant at 200 m and 6 m, respectively. The W_x/W_y ratio for all simulations is 1.00. The Poisson's ratio of the overburden is 10 GPa. Figure 4.9 illustrates S_{max}/D and B/W ratios, and γ as a function of elastic modulus (E). The results show that S_{max}/D ratios, B/W ratios and γ decrease with increasing E. Under the higher E, the S_{max}, B/W and γ under the extraction ratio 40%, 50% and 60% are closely convergent value. The observations are consistent with Ren and Li (2008) and Sartkaew et al. (2018) that the low overburden stiffness would be associated with high magnitude of subsidence, angle of draw and subsidence trough.
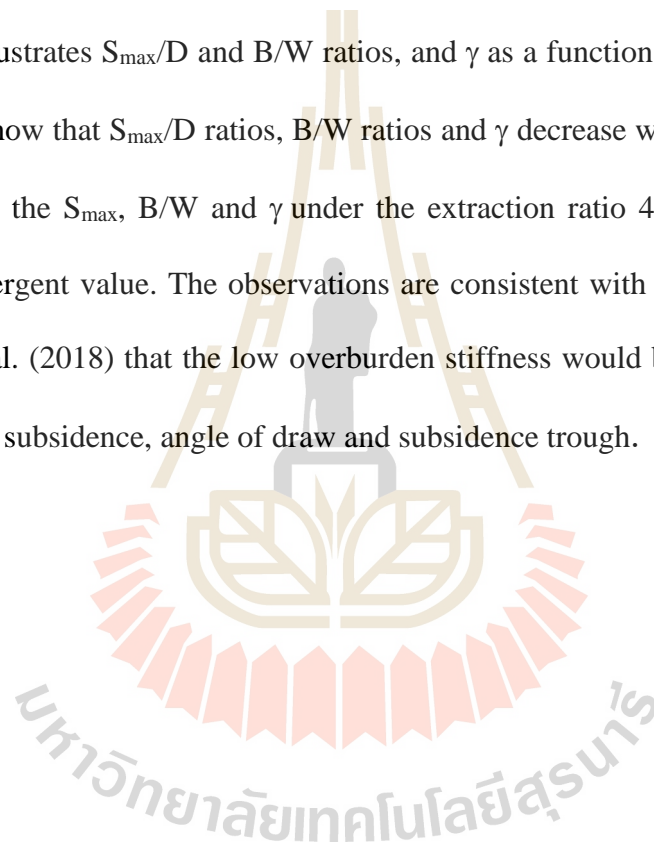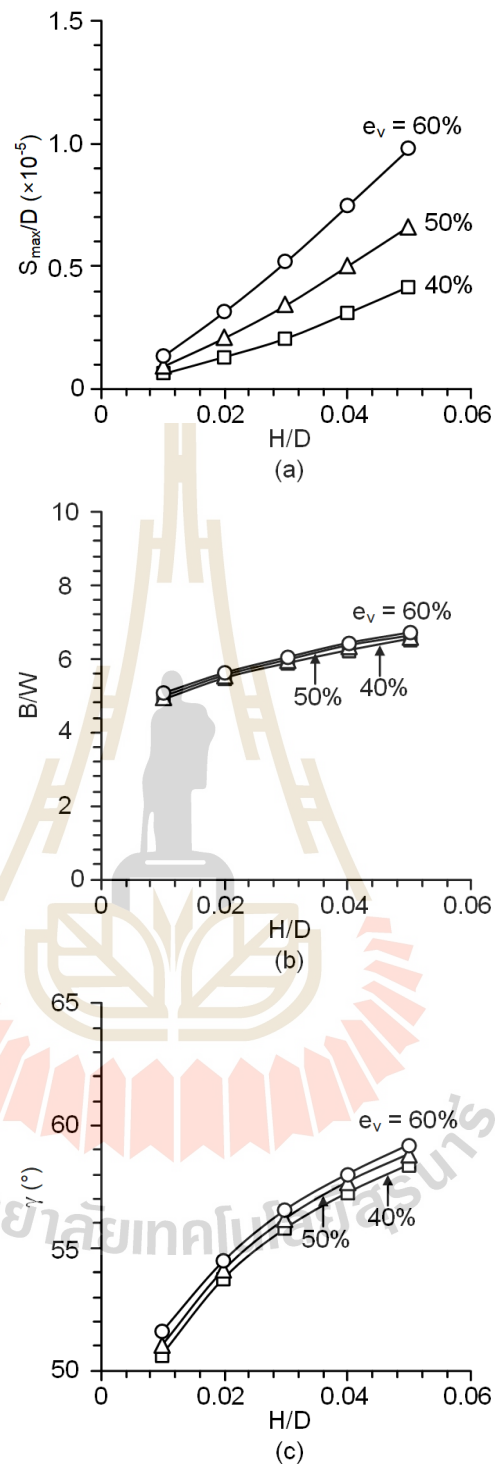
Figure 4.7 (a) Normalized maximum subsidence (S_{max}/D), (b) normalized subsidence

extent (B/W) and (c) angle of draw (γ) as a function of H/D ratios for depth

of 200 m and W_x/W_y ratio at 1.00.
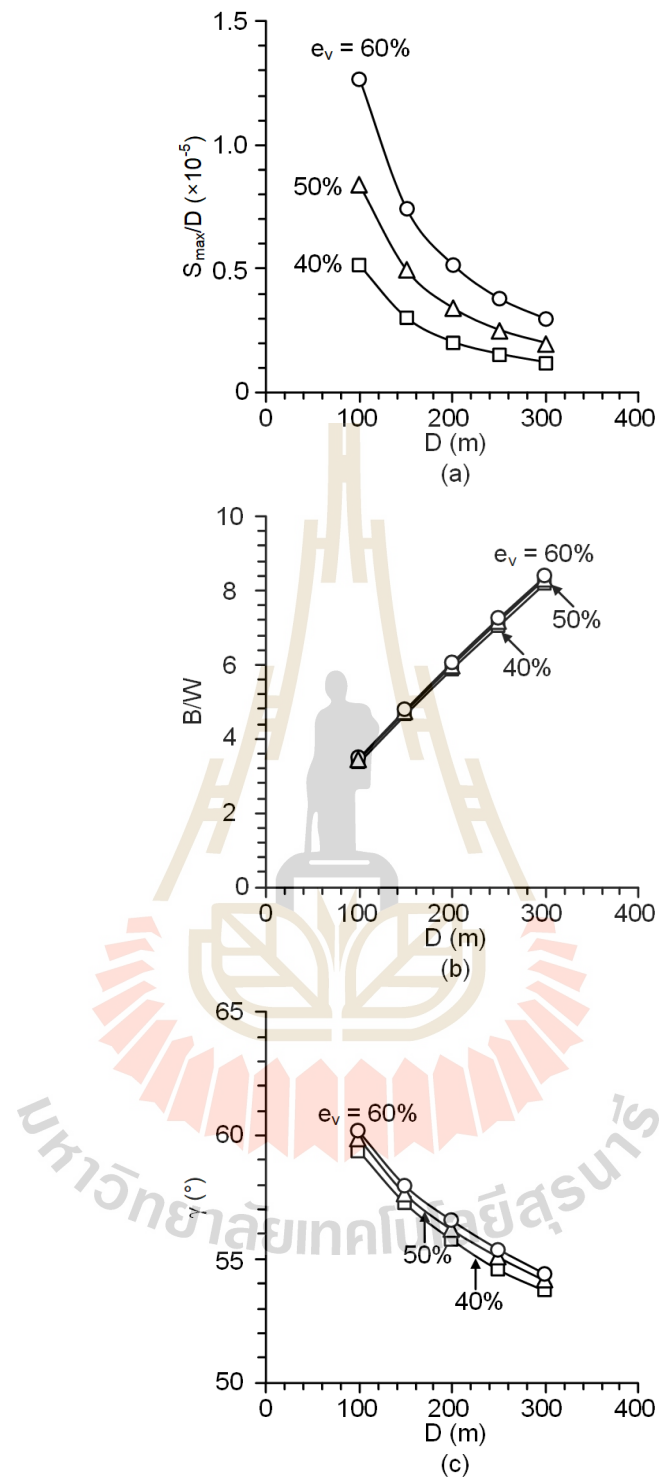
Figure 4.8 (a) Normalized maximum subsidence (S_{max}/D), (b) normalized subsidence

extent (B/W) and (c) angle of draw (γ) as a function of mine depth and

W_x/W_y ratio at 1.00.

Figure 4.9 (a) Normalized maximum subsidence (S_{max}/D), (b) normalized subsidence extent (B/W) and (c) angle of draw (γ) as a function of E for mine depth 200 m.

4.2.6 Effect of abutment pillar

To study the effects of abutment pillar width (barrier pillar, W_{ab}) on surface subsidence, the distances between adjacent mine panels are varied from 25, 50, 75 to 100 m (Figure 4.10). The opening depth and height are constant at 200 m and 6 m, respectively. The panel width (W) and length (L) are constant at 50 m and 100 m. The W_x/W_y ratio for all simulations is 1.00. The elastic modulus of the overburden is 10 GPa. Figure 4.12 shows the normalized subsidence, normalized subsidence trough and angle of draw as a function of W_{ab}/W ratios. The results show that the S_{max}/D ratios decrease, and γ and B/W increase with increasing W_{ab}/W ratios. Lower extraction ratios can reduce the S_{max}, B/W and γ values. These results are in accordance with the principle of superposition that narrower abutment pillar widths cause stresses greatly increase between mine panels (Brady and Brown, 1993), the displacement and subsidence extent from individual panels are overlapped.

Figure 4.10 Abutment pillar width between adjacent mine panels.
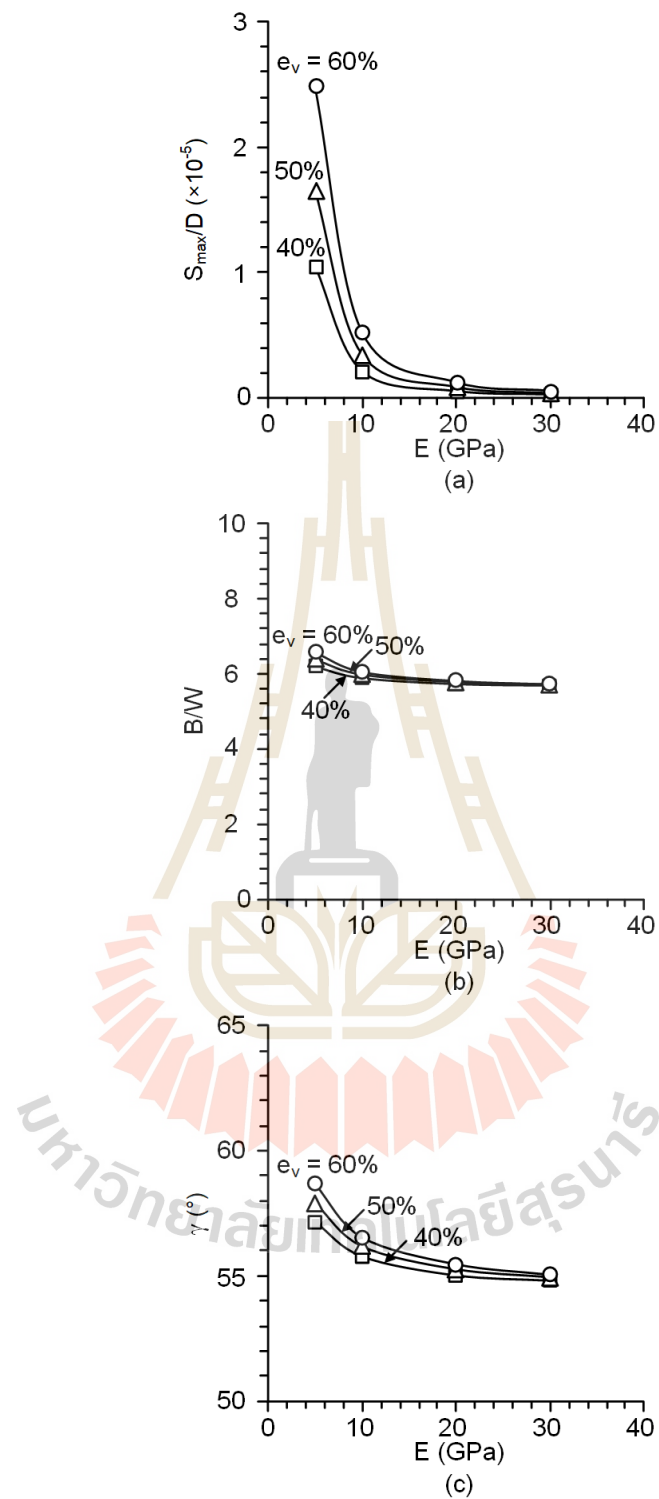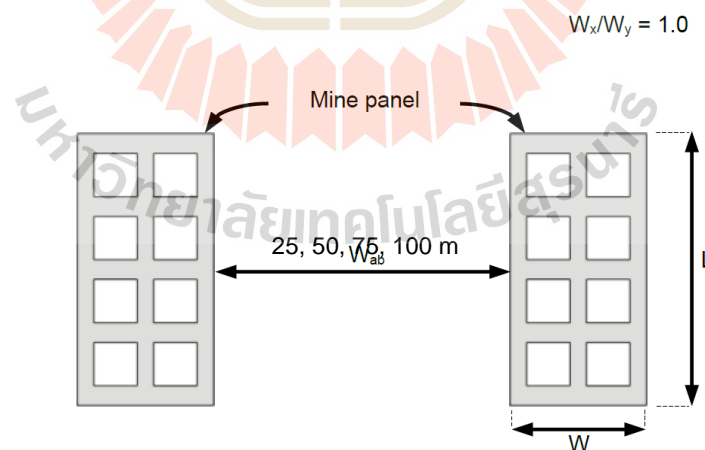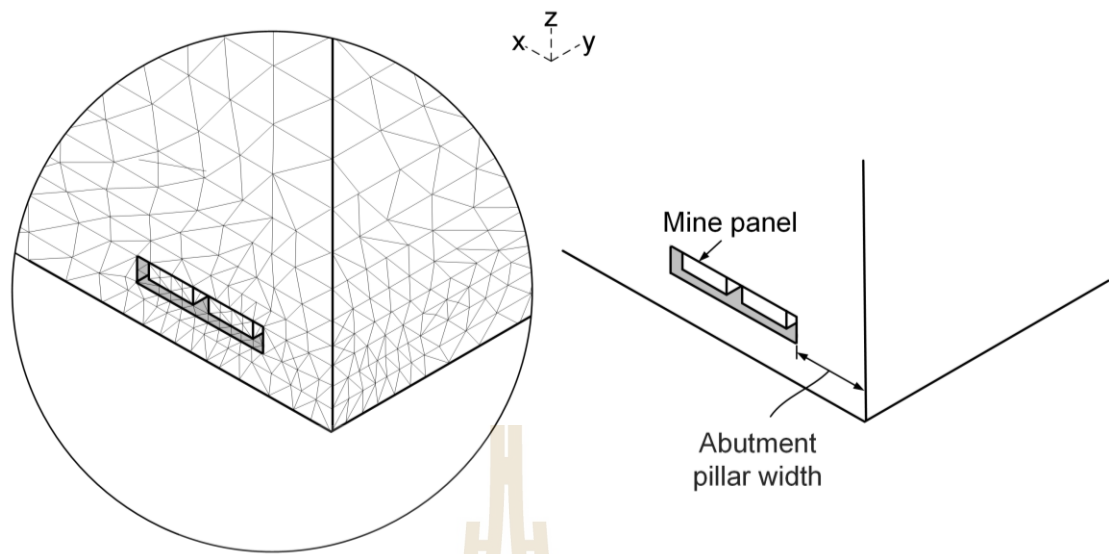
Figure 4.11 Mesh model for SolidWorks simulations.
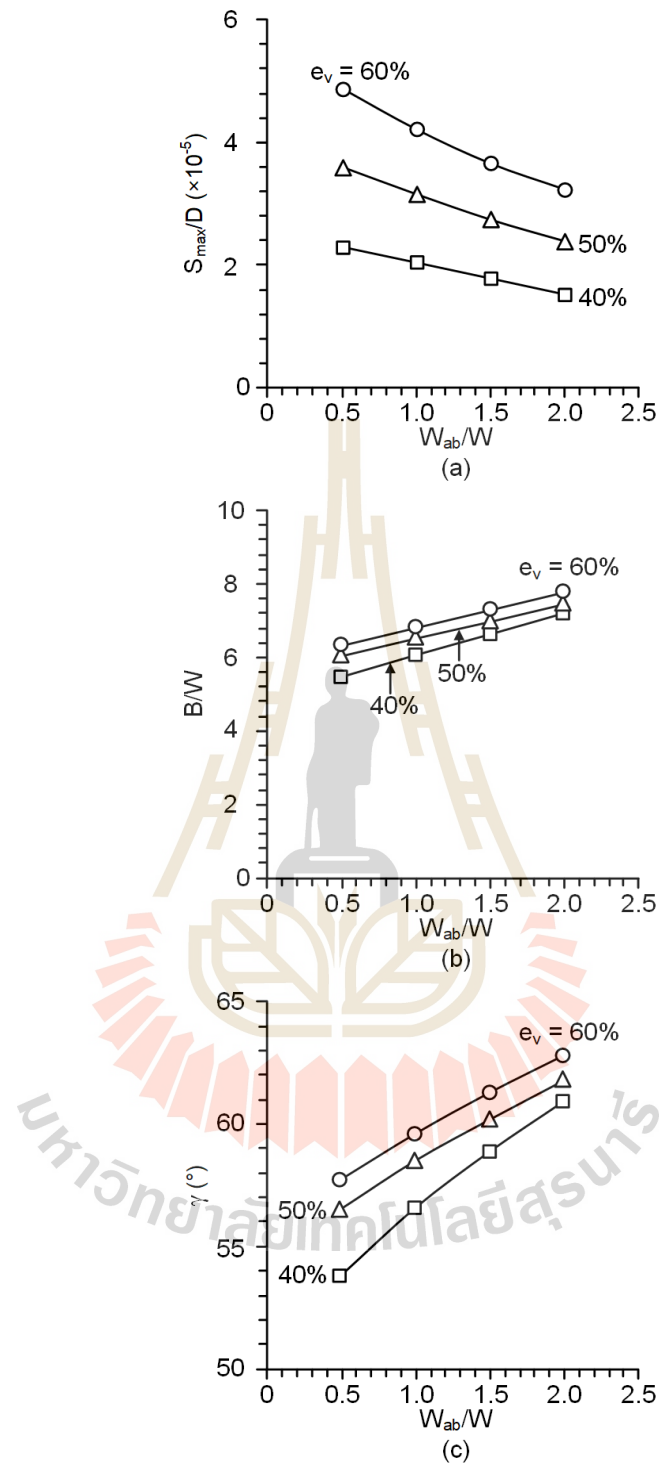
Figure 4.12 (a) Normalized maximum subsidence (S_{max}/D), (b) normalized subsidence

extent (B/W) and (c) angle of draw (γ) as a function of W_{ab}/W ratios.

4.3   Prediction

The mathematical relationships are developed here using the results obtained from three-dimensional computer simulations. The empirical equations can be used to predict the sub-critical surface subsidence components under various opening geometries, overburden properties and extraction ratios. Regression analyses are performed using the SPSS code (Wendai, 2000) to fit the simulation results with the developed empirical equations. The coefficient of correlation (R^2) is an indicator of predictive capability of the equations.

The volumetric extraction ratio (e_v) is first equivalented by the elastic modulus (E). Figure 4.13 (a) plots the normalized maximum subsidence (S_{max}/D) as a function of pillar height which is normalized by the opening depth (H/D). The power relation between the S_{max}/D, H/D and e_v/E ratios can be best represented by:

$$S_{max}/D = 0.256(e_v/E)^{2.224} \cdot (H/D)^{1.3} \qquad (4.2)$$

Where:

E = elastic modulus (GPa)

The empirical constants in the equation above are obtained from the non-linear regression analysis of the computer simulation results. Figure 4.14 compares the predictions with the computer results. The equation is a good correlation with the data, with R^2 at 0.997.

Figure 4.13(b) shows the angle of draw (γ) as a function of pillar height-to-depth ratios (H/D). An empirical equation is presented to predict the angle of draw under various H/D ratios and e_v/E ratios. The equation can be defined as:

$$\gamma = (57.8e_v/E + 74.2)\cdot(H/D)^{0.09} \qquad\qquad \text{(Degrees)} \qquad\qquad (4.3)$$

Figure 4.15 compares the computer results with curve fit in terms of γ as a function of H/D and e_v/E. The relationship between variables is strong, the correlation coefficient (R^2) is 0.987.
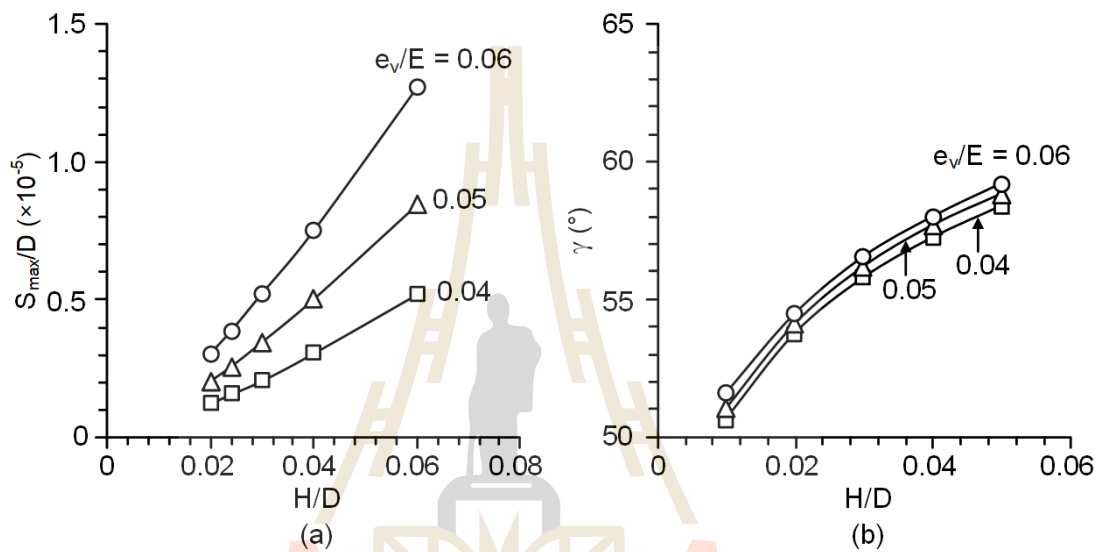
Figure 4.13 Normalized maximum subsidence (S_{max}/D) (a) and angle of draw (b) as a function of pillar height-to-depth ratios (H/D).
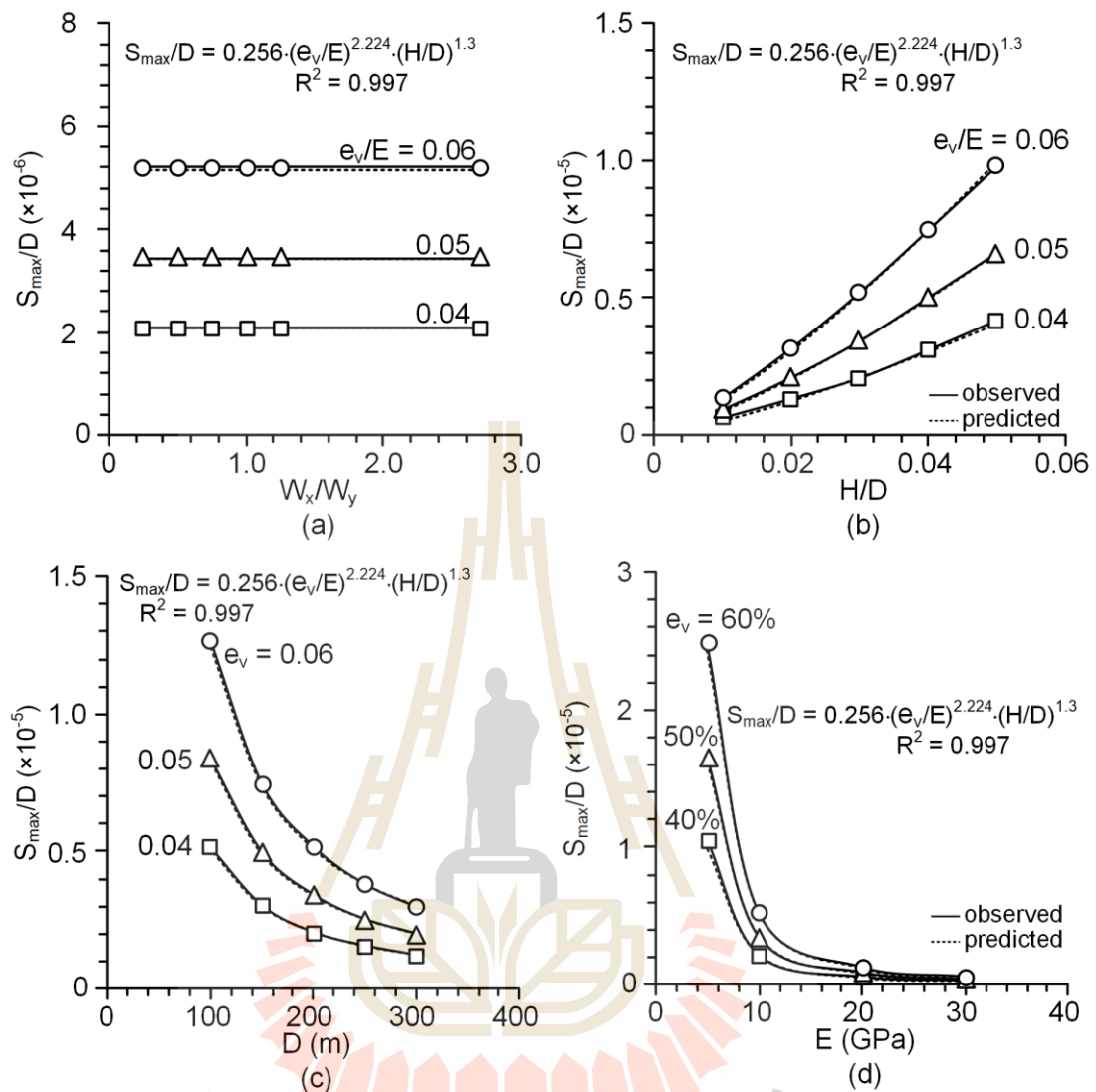
Figure 4.14 Predicted normalized maximum subsidence (S_{max}/D) under various pillar

shapes (a), pillar height-to-depth ratios (b), mine depth (c) and elastic
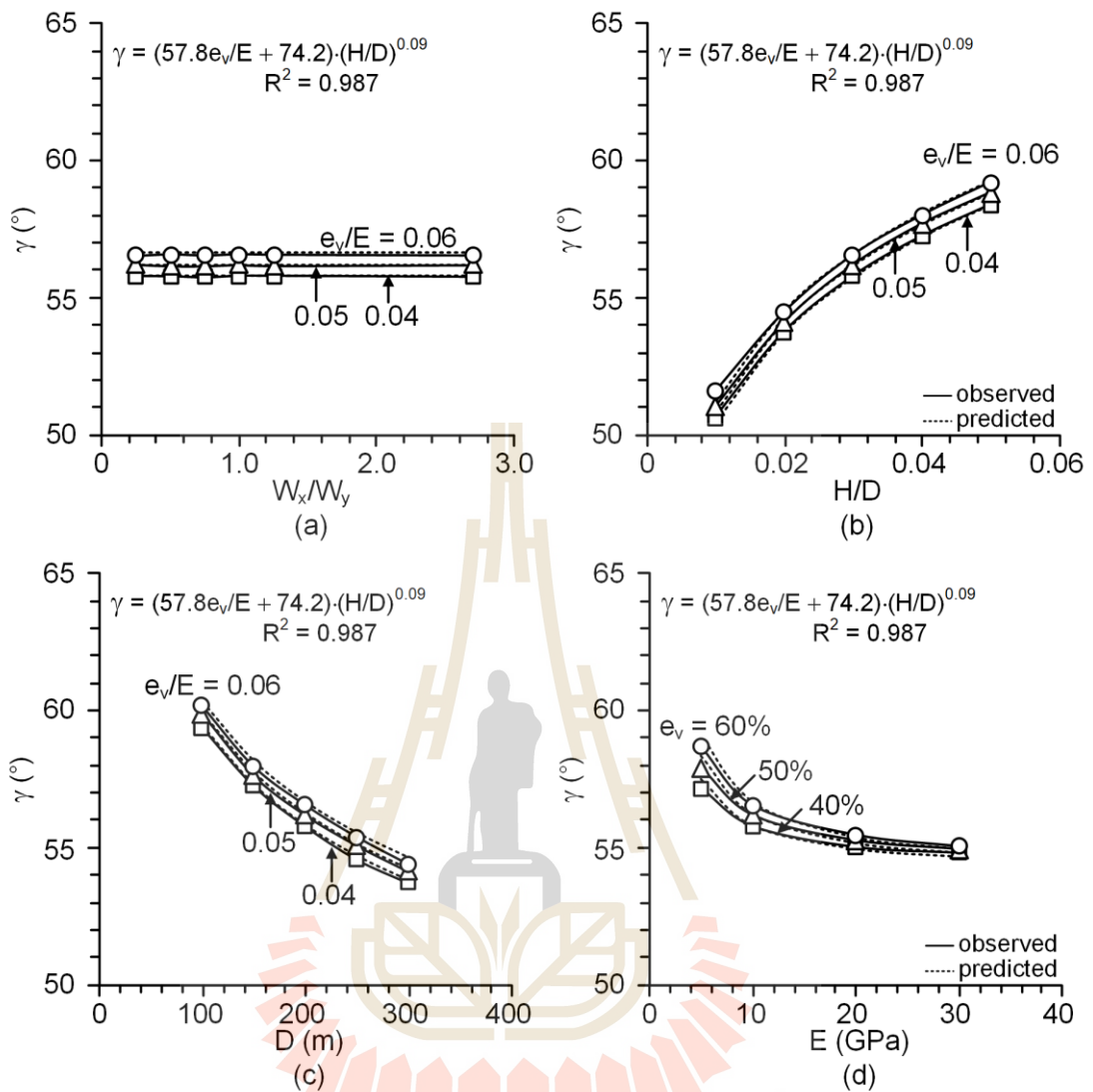
modulus (d).

Figure 4.15 Predicted the angle of draw (γ) under various pillar shapes (a), pillar

height-to-depth ratios (b), mine depth (c) and elastic modulus (d).

CHAPTER V

DISCUSSIONS AND CONCLUSIONS

5.1 Discussions

This study has been focused on subsidence under sub-critical condition, which the extraction width does not exceed 1.0 to 1.4 times of mine depth (Lee and Abel, 1983). Physical and computer simulations are performed to simulate sub-critical surface subsidence induced by underground mining. Both simulations are performed under dry condition. The results indicate that the factors affecting the ground subsidence seem to be the extraction ratio, opening height and depth, and overburden stiffness. The results obtained here agree reasonably well with those from other researchers (Hustrulid, 1976; Yao et al., 1991; Zipf, 2001; Ren and Li, 2008; Tajdus, 2015; Thongprapha et al., 2015; Sartkaew et al., 2018) that the maximum subsidence depends on the size of opening, mine depth and geological conditions. The angle of draw and subsidence trough width are sensitive to mine depth and overburden stiffness. For mining with several mine panels, the subsidence can be determined by the law of superposition. The narrower abutment pillar widths cause stresses greatly increase between mine panels (Brady and Brown, 1993). As a result, the displacement and subsidence extent from individual panels are overlapped.

The proposed empirical equations may be used as a predictive tool to evaluate the maximum surface subsidence and the angle of draw of surface settlement above the opening, based on the opening height and depth, area extraction ratio, and average elastic modulus of the overburden materials under sub-critical condition. Most of

empirical equations proposed by other researchers can predict subsidence components induced by underground opening with only longwall mining or cavity (Singh, 1992; Hawkes, 2010; Thongprapha et al., 2015; Sartkaew et al., 2018). Equations (4.1 and 4.2) are applicable for room-and-pillar method in underground mining, the material with elastic modulus beyond 5 GPa and Poisson's ratio of 0.25 with the extraction ratio does not exceed 70%. As evidenced by the good correlation coefficients ($R^2 > 0.9$) obtained from the proposed empirical equation, the test results are believed to be reasonably reliable. For super-critical subsidence (shallow mining), equation (4.1) can be used to predict maximum subsidence.

5.2 Conclusions

Six test models and seventy-eight numerical models are set up in this study with the same boundary conditions. The synthetic gel is used to simulate the overburden in the physical tests with three geometries of pillar. The computer models use the SolidWorks program.

(1) The results from SolidWorks agree well with the physical model tests. Both methods show that the surface subsidence is not affected by pillar geometries under the same extraction ratio, panel size, opening height, mine depth and elastic modulus.

(2) The maximum subsidence magnitudes are sensitive to opening height, mine depth and elastic properties of overburden. The increasing of mine depth, abutment pillar width, elastic modulus of overburden reduce the maximum subsidence magnitudes. Conversely, the subsidence magnitudes from higher extraction ratios and opening heights are greater than those from lower extraction ratios and opening heights.

(3) The subsidence trough width increases with increasing opening height, depth and abutment pillar width, while decreases with increasing elastic modulus. The subsidence trough is insensitive to the extraction ratio.

(4) The angle of draw increases with increasing opening height and abutment width. The increasing of elastic modulus reduces the angle of draw. The angle of draw is insensitive to the extraction ratio. These results agree with those obtained by Yao et al. (1991), Hustrulid (1976), Zipf (2001), Ren and Li (2008) and Thongprapha et al. (2015).

(5) The results obtained from physical and numerical models under sub-critical subsidence are consistent in terms of the subsidence components under super-critical condition which agree with those obtained by Ren and Li (2008), Thongprapha et al. (2015).

5.3 Recommendations for future studies

The limitations of the boundary conditions and results discussed above lead to suggestions for further research.

(1) The physical and numerical simulations should be performed on irregular pillar shapes within a mine panel to confirm the effects of pillar geometry on surface subsidence components.

(2) The groundwater effect should be considered for physical and numerical simulations.

(3) The overburden strata with different mechanical properties should be investigated to study their relations with the surface subsidence.

REFERENCES

Alejano, L. R., Ramirez-Oyanguren, P., and Taboada, J. (1999). FDM predictive methodology for subsidence due to flat and inclined coal seam mining. **International Journal of Rock Mechanics and Mining Sciences.** 36: 475-491.

Asadi, A., Shahriar, K., Goshtasbi, K., and Najm, K. (2005). Development of new mathematical model for prediction of surface subsidence due to inclined coal-seam mining. **Journal of the South African Institute of Mining and Metallurgy.** 105(1): 15-20.

ASTM D695-15 (2015). **Standard Test Method for Compressive Properties of Rigid Plastics.** Annual Book of ASTM Standards, American Society for Testing and Materials, West Conshohocken, PA.

Brady, B. H. and Brown, E. T. (1993). **Rock Mechanics: for Underground Mining.** Springer science and business media.

Caudron, M., Emeriault, F., Kastner, R., and Al Heib, M. (2006). Sinkhole and soil-structure interaction: Development of an experimental model. In **Proceedings of the Sixth International Conference on Physical Modeling in Geotechnics** (pp. 1261-1267). Hong Kong.

Dassault Systemes. (2017). **Engineering Analysis with SOLIDWORKS Simulation 2017.** SDC publications, Kansas.

Franzius, J. N., Potts, D. M., and Burland, J. B. (2005). The influence of soil anisotropy and K0 on ground surface movements resulting from tunnel excavation. **Geotechnique.** 55(3): 189-199.

Fuenkajorn, K. (2002). Design guideline for salt solution mining in Thailand. **Research and Development Journal of the Engineering Institute of Thailand.** 13(1): 1-8.

Fuenkajorn, K. and Archeeploha, S. (2010). Prediction of cavern configurations from subsidence data. **Engineering Geology.** 110(1-2): 21-29.

Ghabraie, B., Ren, G., and Smith, J. V. (2017). Characterising the multi-seam subsidence due to varying mining configuration, insights from physical modelling. **International Journal of Rock Mechanics and Mining Sciences.** 93: 269-279.

Ghabraie, B., Ren, G., Zhang, X., and Smith, J. (2015). Physical modelling of subsidence from sequential extraction of partially overlapping longwall panels and study of substrata movement characteristics. **International Journal of Coal Geology.** 140: 71-83.

Hawkes, T. P. (2010). A Simple Approach to Subsidence Prediction Above Longwall Mines. **PhD. dissertation**. Brigham Young University, Utah, United States.

Hill, D. (2015). Coal pillar design criteria for surface protection. In **Proceedings of the Coal Operators' Conference** (pp. 31–38). Wollongong, Australia.

Hustrulid, W. A. (1976). A review of coal pillar strength formulas. **Rock Mechanics.** 8(2): 115-145.

Jenkunawat, P. (2007). Results of drilling to study occurrence of salt cavities and surface subsidence Ban Non Sabaeng and Ban Nong Kwang, Sakon Nakhon.

In **Proceedings of the First Thailand Symposium on Rock Mechanics.** Suranaree University of Technology, Thailand.

Lee, F. T. and Abel, J. F. (1983). **Subsidence from Underground Mining; Environmental Analysis and Planning Considerations (No. 876).** US Geological Survey.

Li, X. Q. and Zhu, C.C. (2007). Numerical analysis on the ground settlement induced by shield tunnel construction. **Journal of Highway and Transportation Research and Development**. 2(2): 73-79.

Mark, C. (2006). The evolution of intelligent coal pillar design: 1981–2006. In **Proceedings of the Twenty-fifth international conference on ground control in mining** (pp. 325-334). West Virginia University, West Virginia.

Meesook, A. (2011). Cretaceous. **The Geology of Thailand**. Geological Society, London.

Meguid, M. A., Saada, O., Nunes, M. A., and Mattar, J. (2008). Physical modeling of tunnels in soft ground: a review. **Tunnelling and Underground Space Technology.** 23(2): 185-198.

National Coal Board, 1975. **Subsidence Engineers Handbook**. National Coal Board. London. 401 p.

Nikolić, M., Roje-Bonacci, T., and Ibrahimbegović, A. (2016). Overview of the numerical methods for the modelling of rock mechanics problems. **Tehnicki Vjesnik-Technical Gazette.** 23(2): 627-637.

Parise, M. and Lollino, P. (2011). A preliminary analysis of failure mechanisms in karst and man-made underground caves in Southern Italy. **Geomorphology.** 132–143.

Park, D. W. and Li, J. (2004). Subsidence simulation using laser optical triangulation distance measurement devices. In **Proceedings of the Sixth Gulf Rocks, North America Rock Mechanics Symposium (NARMS)**. American Rock Mechanics Association. Houston, Texas.

Poulsen, B. A. and Shen, B. (2013). Subsidence risk assessment of decommissioned bord-and-pillar collieries. **International Journal of Rock Mechanics and Mining Sciences.** 60: 312-320.

Rajabi, A. M. (2018). A numerical study on land subsidence due to extensive overexploitation of groundwater in Aliabad plain, Qom-Iran. **Natural Hazards.** 93(2): 1085-1103.

Reddish, D. J. (1989). The modeling of rock mass behaviour over large excavations using non-linear finite element techniques. **Mining Department Magazine, University of Nottingham.** 41: 93-102.

Ren, G. and Li, J. (2008). A study of angle of draw in mining subsidence using numerical modeling techniques. **Electronic Journal of Geotechnical Engineering.** 13: 1-14.

Rocscience Inc. (2001). **Phase2 User's Guide**. Itasca Consulting Group Inc., Toronto, Canada.

Saoanunt, N. and Fuenkajorn, K. (2015). Physical model simulations of super-critical subsidence as affected by mining sequence and excavation rate. In **Proceedings of the Ninth South East Asia Technical University Consortium Symposium (SEATUC).** Suranaree University of Technology, Thailand.

Sartkaew, S. and Fuenkajorn, K. (2016). Verifications of empirical method and numerical simulation using physical model for subsidence prediction of Maha sarakham formation. **Engineering Journal of Research and Development**, 27(3): 17-27.

Sartkaew, S., Khamrat, S., and Fuenkajorn, K. (2018). Physical model simulation of surface subsidence under sub-critical condition. **International Journal of Physical Modelling in Geotechnics.** 19(5): 234-246.

Satarugsa, P., Youngmee, W., and Meesawat, S. (2005). New regional boundary of Maha Sarakham Formation in the northeastern Thailand: results from 2D seismic mapping. In **Proceedings on International Conference on Geology, Geotechnology and Mineral Resources of Indochina (GEOINDO 2005)**. Khon Kaen University, Thailand.

Shahriar, K., Amoushahi, S., and Arabzadeh, M. (2009). Prediction of surface subsidence due to inclined very shallow coal seam mining using FDM. In **Proceedings of the Coal Operators Conference** (pp. 130-139). University of Wollongong, Dubai, United Arab Emirates.

Singh, M. M. (1992). Mine subsidence. In: Hartman, H.L. (Ed.), **SME Mining Engineering Handbook** (pp. 938–971). Society for mining metallurgy and exploration, Littleton, Colorado.

Tajduś, K. (2015). Numerical modelling of the mining induced horizontal displacement. **Studia Geotechnica et Mechanica.** 37(4): 65-73.

Thongprapha, T., Fuenkajorn, K., and Daemen, J. J. K. (2015). Study of surface subsidence above an underground opening using a trap door apparatus. **Tunnelling and Underground Space Technology.** 46: 94-103.

Wannakao, L., Munjai, D., and Janyakorn, S. (2005). Geotechnical investigation of surface subsidence at Ban Non Sabaeng salt production area, Sakon Nakhon, Thailand. In **Proceedings of the International Conference on Geology, Geotechnical and Mineral Resources of Indochina**. Khon Kaen University, Thailand.

Wendai, L. (2000). **Regression Analysis, Linear Regression and Profit Regression, In 13 Chapters; SPSS for Windows: Statistical Analysis.** Publishing House of Electronics Industry, Beijing, China.

Whittaker, B. N. and Reddish, D. J. (1989). **Subsidence Occurrence, Prediction and Control**. Amsterdam: Elsevier Science Publishers.

Wu, J., Shi, X., Ye, S., Xue, Y., Zhang, Y., Wei, Z., and Fang, Z. (2010). Numerical simulation of viscoelastoplastic land subsidence due to groundwater overdrafting in Shanghai, China. **Journal of Hydrologic Engineering.**15(3): 223-236.

Yao, X. L., Reddish, D. J., and Whittaker, B. N. (1991). Influence of overburden mass behavioural properties on subsidence limit characteristics. **Mining Science and Technology.** 13(2): 167-173.

Yu, Y., Chen, S. E., Deng, K. Z., and Fan, H. D. (2017). Long-term stability evaluation and pillar design criterion for room-and-pillar mines. **Energies.** 10(10).

Zhou, Q. C. (2006). Study on the Mechanical Property of a Sandstone under Geothermal-mechanical and Hydraulic Mechanical Coupling. **PhD. dissertation**. Institute of Rock and Soil Mechanics, Chinese Academy of Sciences, China.

Zipf Jr, R. K. (2001). Toward pillar design to prevent collapse of room-and-pillar mines. In **Proceedings of the One Hundred Eighth Annual Exhibit and Meeting.** National Institute for Occupational Safety and Health, Colorado.
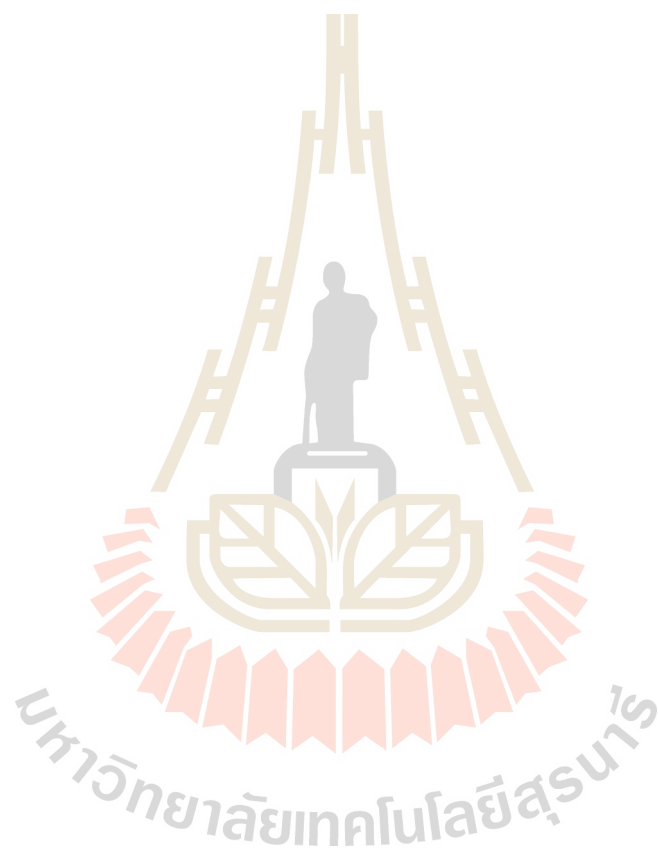
BIOGRAPHY

Miss Thitawee Sooppattagul was born on May 5, 1995 in Surin Province, Thailand. She received her Bachelor's Degree in Engineering (Geological Engineering) from Suranaree University of Technology in 2017. For her post-graduate, she continued to study with a Master's degree in Civil, Transportation and Geo-resources Engineering Program, Institute of Engineering, Suranaree University of Technology. During graduation, 2017-2019, she was a part time worker in position of research assistant at the Geomechanics Research Unit, Institute of Engineering, Suranaree University of Technology.